

Geochemistry, Geophysics, Geosystems®






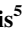









RESEARCH ARTICLE

10.1029/2024GC011563

Crustal Heterogeneity Onshore Central Spitsbergen: Insights From New Gravity and Vintage Geophysical Data

Special Collection:

Through the Arctic Lens:
Progress in Understanding the
Arctic Ocean, Margins and
Landmasses

Kim Senger^{1,2} , Fenna Ammerlaan^{1,3} , Peter Betlem^{1,4} , Marco Brønner⁵,
Marie-Andrée Dumais⁵ , Jomar Gellein⁵, Tormod Henningsen¹⁷, Julian Janocha^{1,6} ,
Erik P. Johannessen⁷ , Jonas Liebsch^{1,8} , Jakob Machleidt^{1,9}, Tereza Mosočiová^{1,10,11} ,
Snorre Olaussen¹ , Bo Olofsson¹², Nil Rodes¹ , Sofia Rylander^{1,12}, Grace E. Shephard^{13,14} ,
Aleksandra Smyrak-Sikora¹⁵ , Juan D. Solano-Acosta^{1,16}, and Anna Sterley^{1,11} 

Key Points:

- New gravity data acquired onshore Spitsbergen, with 260 stations acquired along seven profiles with a cumulative length of 329 km
- The gravity profiles compare well with vintage regional data from the 1980s but provide much higher resolution along the profiles
- Interpretation indicates a sedimentary foreland basin, a basement high and laterally varying basement composition

¹Department of Arctic Geology, The University Centre in Svalbard, Longyearbyen, Norway, ²Geodynamics of the Polar Regions, Department of Geosciences, University of Bremen, Bremen, Germany, ³Department of Earth Sciences, Utrecht University, Utrecht, The Netherlands, ⁴Now at Norwegian Geotechnical Institute, Oslo, Norway, ⁵Geological Survey of Norway, Trondheim, Norway, ⁶Department of Geosciences, UiT—The Arctic University of Norway, Tromsø, Norway, ⁷Skolithos, Stavanger, Norway, ⁸Institute of Earth Sciences, University of Iceland, Reykjavik, Iceland, ⁹Geocenter Northern Bavaria, Friedrich-Alexander University Erlangen-Nuremberg, Erlangen, Germany, ¹⁰Masaryk University, Brno, Czechia, ¹¹Department of Geosciences, The University of Oslo, Oslo, Norway, ¹²KTH Royal Institute of Technology, Stockholm, Sweden, ¹³Department of Geosciences, Centre for Planetary Habitability, University of Oslo, Oslo, Norway, ¹⁴Research School of Earth Sciences, Australian National University, Canberra, NSW, Australia, ¹⁵Department of Geosciences, Norwegian University of Science and Technology, Trondheim, Norway, ¹⁶Tallinn University of Technology, Tallinn, Estonia, ¹⁷Retired, Harstad, Norway

Correspondence to:

K. Senger,
kims@unis.no

Citation:

Senger, K., Ammerlaan, F., Betlem, P., Brønner, M., Dumais, M.-A., Gellein, J., et al. (2025). Crustal heterogeneity onshore central Spitsbergen: Insights from new gravity and vintage geophysical data. *Geochemistry, Geophysics, Geosystems*, 26, e2024GC011563. <https://doi.org/10.1029/2024GC011563>

Received 9 MAY 2024
Accepted 19 NOV 2024

Author Contributions:

Conceptualization: Kim Senger, Tormod Henningsen, Snorre Olaussen
Data curation: Peter Betlem, Jakob Machleidt, Nil Rodes
Formal analysis: Kim Senger, Fenna Ammerlaan, Marie-Andrée Dumais, Jomar Gellein, Sofia Rylander, Juan D. Solano-Acosta, Anna Sterley
Funding acquisition: Kim Senger, Julian Janocha, Sofia Rylander, Anna Sterley

© 2025 The Author(s). *Geochemistry, Geophysics, Geosystems* published by Wiley Periodicals LLC on behalf of American Geophysical Union.

This is an open access article under the terms of the [Creative Commons Attribution License](https://creativecommons.org/licenses/by/4.0/), which permits use, distribution and reproduction in any medium, provided the original work is properly cited.

Abstract Gravity data provide constraints on lateral subsurface density variations and thus provide crucial insights into the geological evolution of the region. Previously, gravity data from the Norwegian Arctic archipelago of Svalbard comprised an onshore regional gravity database with coarse station spacing of 2–20 km, offshore gravity profiles acquired in some fjords, airborne gravity, and satellite altimetry. The sparse regional point-based onshore coverage hampered the direct integration of gravity data with seismic profiles acquired onshore Svalbard in the late 1980s and early 1990s. In April 2022, we acquired gravity data at 260 new stations along seven profiles from western to eastern Spitsbergen, with a cumulative length of 329 km. The profiles were acquired directly along selected seismic profiles and provide much closer station spacing (0.5–2 km) compared to the regional inland grid (2–20 km) acquired in the late 1980s (total number of onshore stations: 1,037). Having processed the data, we compared the first-order density trends of our new data with the legacy regional grid. The new gravity data are consistent with the regional data, imaging a gravity low in the western part of the area underlying a foreland basin and a gravity high in the northwestern part of the area likely associated with a basement high or denser basement. We compare the new and vintage gravity using maps and profiles, linked to the known major tectonic features such as major basinal axes and fault zones, as well as other geophysical data sets including seismics and magnetics.

Plain Language Summary Gravity data inform us about the density structure below the ground level. The density structure provides information on the extent of sedimentary basins, basement highs and other features with contrasting density to its surroundings. Together with other parameters (such as velocity and magnetic susceptibility), gravity data can constrain the architecture of the shallow to deep subsurface. In this paper, we focus on the high Arctic archipelago of Svalbard, specifically its largest island, Spitsbergen. Gravity data were acquired onshore Svalbard in the late 1980s, both from the ground, boats and airplanes. In April 2022, we collected new ground-based gravity data onshore Svalbard using snowmobiles. The motivation of the survey was to improve seismic interpretation along several profiles across Spitsbergen. We acquired new gravity data at 260 stations along the seven profiles totaling 329 km. We have compared the new data with pre-existing gravity data collected in a much coarser grid, and found good overlap between the data. The subsurface density structure from the gravity data is compared to regional geology. A major sedimentary basin is clearly evident from the new gravity data, as is a basement high.

Investigation: Kim Senger, Jomar Gellein, Tormod Henningsen, Julian Janocha, Tereza Mosoćiová, Bo Olofsson, Nil Rodes, Sofia Rylander, Anna Sterley

Methodology: Kim Senger

Project administration: Kim Senger

Resources: Kim Senger, Peter Betlem, Tormod Henningsen

Supervision: Kim Senger

Visualization: Kim Senger, Grace E. Shephard, Aleksandra Smyrak-Sikora

Writing – original draft: Kim Senger

Writing – review & editing: Kim Senger, Fenna Ammerlaan, Peter Betlem, Marco Brönnert, Marie-Andrée Dumais, Tormod Henningsen, Julian Janocha, Snorre Olaussen, Grace E. Shephard, Aleksandra Smyrak-Sikora, Juan D. Solano-Acosta

1. Introduction

Understanding the subsurface structure and physical composition of a region is critical to decipher its geological evolution and to place it in a regional geodynamic setting. Constraints on the subsurface can be achieved via numerous direct and indirect geophysical methods and related properties, including density, magnetic susceptibility, temperature (heat flow), and acoustic impedance (i.e., seismic).

Gravity anomaly data are a type of potential field data and provide important constraints in identifying and characterizing major structural features where subsurface density contrasts occur. Such settings include sedimentary basins (Døssing et al., 2014), major mountain belts (ten Brink et al., 1997), and the seafloor beneath ice shelves (Muto et al., 2013). Gravity can also be used to constrain a region's lithospheric thickness (Zhao et al., 2012) and mantle viscosity (Bagherbandi et al., 2022). The measured variability in gravitational acceleration is a signal of density contrasts situated in both the crust and the mantle.

1.1. Geophysical Exploration of Svalbard—A Window to the Circum-Arctic

The Svalbard archipelago is located at the north-west corner of the continental Barents Shelf, close to the North Atlantic-Arctic Ocean mid-ocean spreading systems (Figure 1). Svalbard is currently uplifting (Kierulf et al., 2022; Lasabuda et al., 2021), with its exposed onshore geology testifying to its long-term and dynamic evolution and its relation to the wider Arctic region (e.g., Pease et al., 2014; Petrov et al., 2016).

For over a century, Svalbard has attracted geoscientists trying to decipher its connection to Arctic Canada, Greenland, and Russia and the Arctic's partly shared geological evolution. Several tectonic events recognized in Svalbard also affected the wider Arctic and North Atlantic regions (Figure 1), creating the present-day tectonic elements and crustal architecture (Figure 2). These include the Caledonian orogeny (i.e., Barentsian Caledonides in Gee et al., 2006), Devonian orogenic collapse basins (Braathen et al., 2018; Piepjohn, 2000), Late Devonian/Early Carboniferous Ellesmerian compressional deformation (locally referred as the Svalbardian phase; Bergh et al., 2011; Piepjohn, 2000), Mid-Late Carboniferous rifting of the Barents Shelf (Faleide et al., 2008; Johannessen & Steel, 1992; Smyrak-Sikora et al., 2021), Early Cretaceous circum-Arctic magmatism associated with the High Arctic Large Igneous Province (HALIP; Maher, 2001; Senger et al., 2014), and Paleogene Eurekan plate reorganizations and formation of a fold-thrust belt (Braathen et al., 1999; Faleide et al., 2008; Piepjohn et al., 2016). Oligocene transtensional structures in Svalbard (e.g., Gabrielsen et al., 1992; Schaaf et al., 2021) are related to the development of the Fram Strait, an important oceanographic connection between the Arctic Ocean and the North Atlantic (Faleide et al., 2008; Lasabuda et al., 2018; Straume et al., 2020).

Until relatively recently, a major geoscientific focus of Svalbard was its value as an analogue for the petroleum provinces of the south-western Barents Sea (e.g., Nøttvedt et al., 1993; Olaussen et al., 2024; Worsley, 2008). Petroleum exploration onshore Svalbard resulted in the drilling of 18 exploration boreholes from 1961 to 1994 (Senger et al., 2019) and onshore-offshore 2D reflection seismic data acquisition campaigns largely in the 1980s–1990s (Eiken, 1994). Seismic interpretation of these profiles is hampered by high acoustic velocities of the uplifted sediments, hard seabed reflections in the fjords, and the presence of acoustically heterogeneous permafrost onshore. Deeper reflectors are notably difficult to interpret. There are only a few refraction seismic profiles located along the continental margin to the west (e.g., Ritzmann et al., 2002; Figure 3). It follows that the regional lithospheric structure of Svalbard is poorly constrained compared to its surrounding continental margins. Additional non-seismic data are required to both constrain the seismic interpretation and permit an understanding of the broader evolution of Svalbard and, specifically, its crustal structure.

Gravity data were acquired in and around Svalbard since the 1980s, with an initial geographic focus on the tectonically sheared margin offshore western Svalbard (Table 1; Figure 2). Surveys were mostly conducted offshore, often integrated with magnetic, seismic refraction, and heat flow profiles. Gravity data are available along eight marine profiles and 1,037 onshore gravity stations acquired in the late 1980s–early 1990s (Table 1; Figure 3). The regional gravity compilation (Figure 2b; Olesen et al., 2010) is dominated by a gravity low in western Spitsbergen, corresponding to a Paleogene foreland basin filled with sediments with a lower density compared to the surrounding and underlying basement rocks (Figure 2a). An elongated north-south striking gravity high in northern Spitsbergen coincides with the extension of the Billefjorden Fault Zone. A less pronounced gravity high in north-eastern Svalbard (Nord-austlandet) spatially co-incides with pre-Caledonian basements intruded by Caledonian-age granites and covered by the Austfonna ice sheet (Figure 2). This

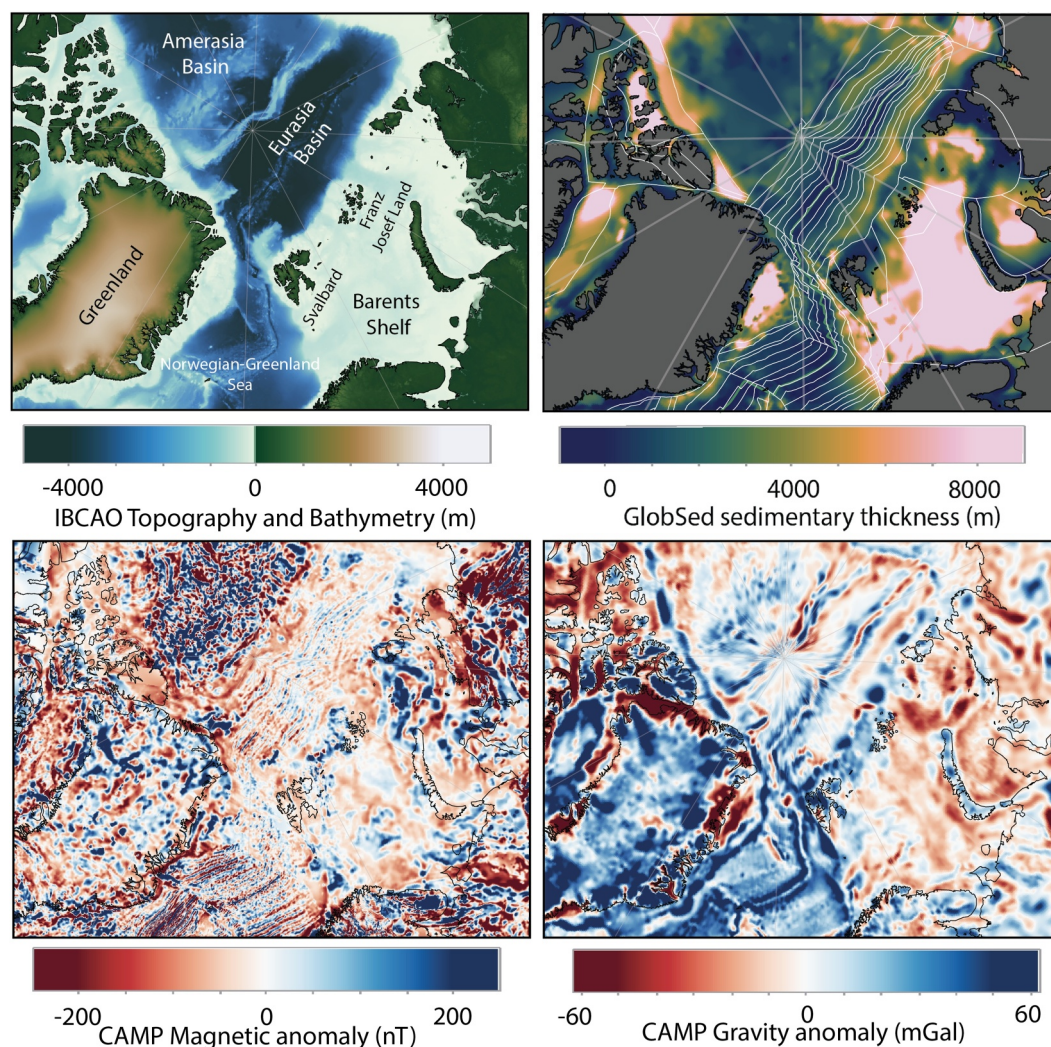


Figure 1. Arctic setting of Svalbard—topography and bathymetry (IBCAO map (Jakobsson et al., 2012)), sedimentary thickness overlain with tectonic domains (GlobSed Straume et al., 2019; adapted from Müller et al., 2019), CAMP magnetic anomaly map and gravity anomaly map (CAMP—Gaina et al., 2011). Coastlines in black. Perceptually uniform color maps from Cramer et al. (2020) are used throughout the manuscript where possible. CAMP = Circum-Arctic mapping project.

gravity high continues south toward Edgeøya where its origin is enigmatic. Both of these dominate the gravity structure in the study area. However, the data coverage is rather sparse, especially in inland areas (ca. 20 km spacing between gravity stations).

To constrain the density structure of the subsurface, a denser network of gravity profiles is required onshore compared to the regional survey from the 1980s. Ideally, this network is spatially aligned with complementary data, notably seismic reflection profiles and geological maps that facilitate joint interpretation through data integration. Furthermore, while the margins west and north of Svalbard and the Barents Sea to the south-east have received considerable attention in terms of characterizing subsurface density structures, onshore Svalbard has been largely overlooked (Figure 3).

Central Spitsbergen is an important study site where the geological structures are relatively well known but not yet fully characterized in depth. Understanding the crustal architecture in this area is not only important to decipher the geological evolution but is also of societal relevance, in particular given the ongoing characterization of the geothermal potential of this most populated area of Svalbard (Senger et al., 2023).

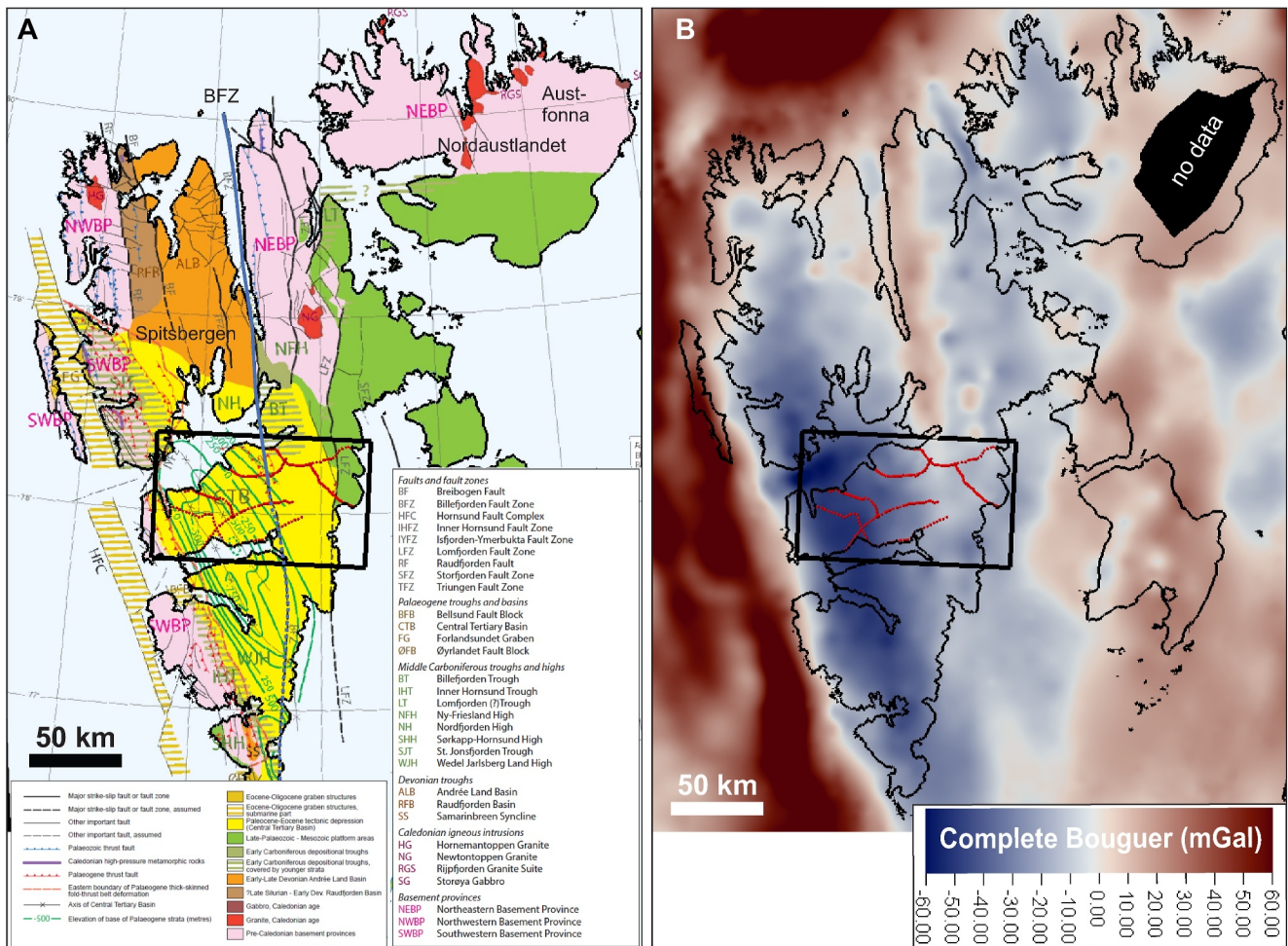


Figure 2. Regional geological setting and gravity data over the study area (black rectangle, red points indicate actual measured locations). (a) Structural element map of Spitsbergen from Dallmann (2015). The main axis of the Central Spitsbergen Basin (here labeled CTB), the Billefjorden Fault Zone (BFZ) and the Lomfjorden Fault Zone (LFZ) is digitized on this map and used subsequently to place the gravity data in perspective. (b) Complete Bouguer gravity anomaly map, data from Olesen et al. (2010). The maps are projected in UTM33N, ED50 datum.

1.2. Motivation for and Design of an Onshore Gravity Survey

We designed an onshore gravity survey covering large parts of central Spitsbergen, and acquired the data in April 2022. The motivation for this survey was to provide information on subsurface density distribution along a series of regional 2D seismic profiles acquired onshore Spitsbergen in the late 1980s and early 1990s as part of petroleum exploration (Eiken, 1985, 1994; Nøttvedt et al., 1993; Senger et al., 2019). The planned gravity stations were aligned along the seismic profiles. Station spacing of 0.5–2 km was planned to improve the imaging of anomalies over the existing regional grid compiled from stations with irregular spacing of ca 5–10 km in the inland areas.

In summary, the survey's main motivation was three-fold: (a) obtain higher-resolution gravity profile data than previously existed, (b) improve the understanding of the study area's crustal structure, and (c) constrain regional-scale seismic interpretations, particularly at depth.

In this contribution, we review existing geophysical studies in and around Svalbard, focusing on gravity anomalies as well as seismic refraction, magnetic, and electromagnetic profiling. We subsequently present new gravity data (260 stations) acquired along 7 profiles (cumulative length 329 km) onshore Spitsbergen. Specifically, we outline the survey planning, data acquisition and gravity data processing. Furthermore, we compare the newly acquired data with the regional gravity grid (Olesen et al., 2010), largely based on regional surveying in the 1980s–1990s. Finally, we discuss the overall trends in the gravity data with respect to first-order geological

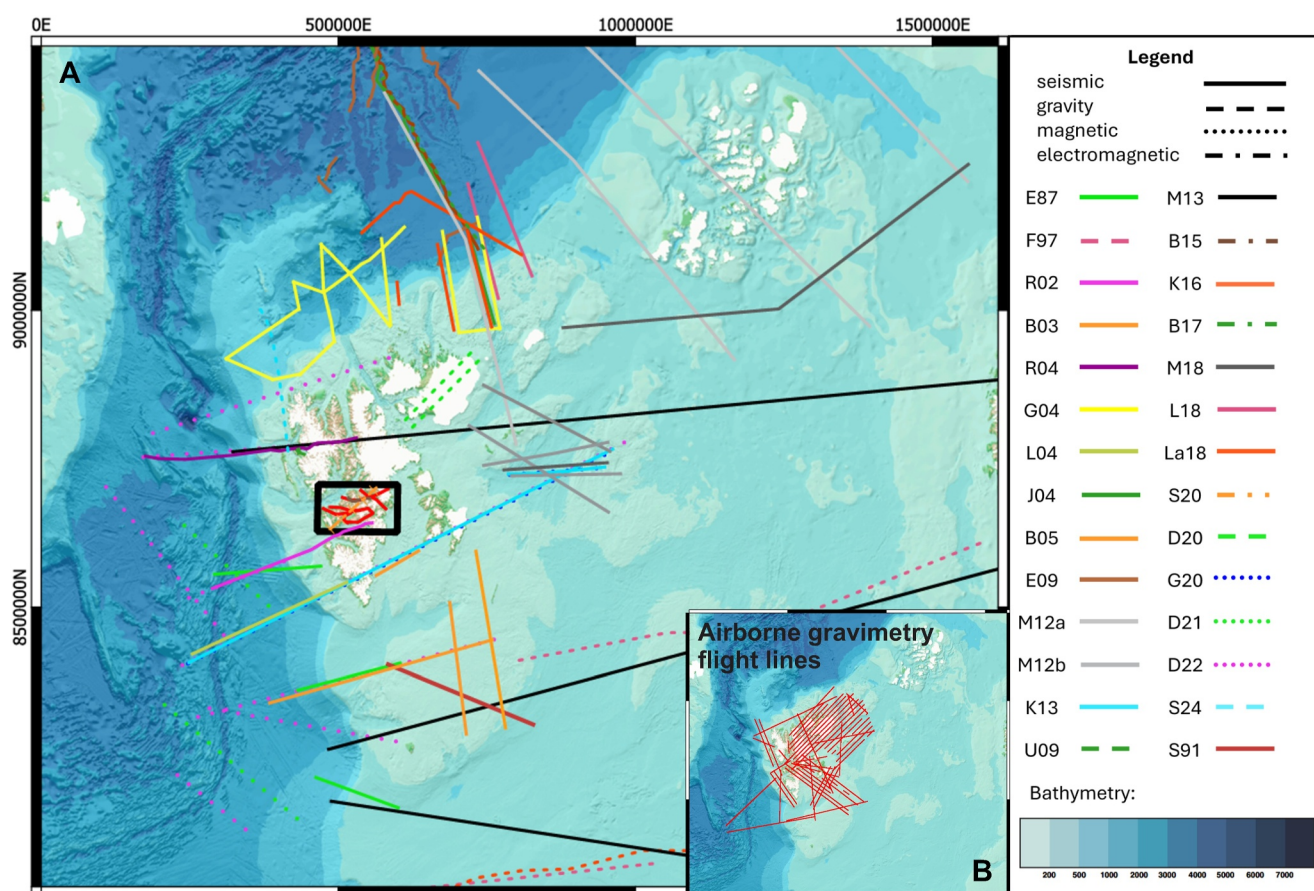


Figure 3. (a) Outline of the spatial coverage of crustal-scale geophysical studies in and around Svalbard and the study area (black rectangle). Refer to Table 1 for the details of the various studies. (b) Same plot as (a) but indicating the past gravity acquisition onshore (blue points) and aerial (red lines). (c) Same plot as (a) but illustrating the seismic data coverage in the area (white lines). Note that not all seismic lines in the area are openly available. Legend corresponds to the IDs and further details of studies in Table 1: E87 = Eldholm et al. (1987); F97 = Fichler et al. (1997); R02 = Ritzmann et al. (2002); B03 = Breivik et al. (2003); R04 = Ritzmann et al. (2004); G04 = Geissler and Jokat (2004); L04 = Ljones et al. (2004); J04 = Jokat and Micksch (2004); B05 = Breivik et al. (2005); Engen et al. (2009); M12a = Minakov et al. (2012a); M12b = Minakov et al. (2012b); K13 = Krysinski et al. (2013); M13 = Marelllo et al. (2013); B15 = Beka et al. (2015); K16 = Klitzke et al. (2016); B17 = Beka et al. (2017a, 2017b); M18 = Minakov et al. (2018); L18 = Lutz et al. (2018); La18 = Lasabuda et al. (2018); S20 = Selway et al. (2020); D20 = Dumais and Bronner (2020); G20 = Grad and Majorowicz (2020); D21 = Dumais et al. (2021); D22 = Dumais et al. (2022). S24 = Smelror et al. (2024).

structures reflecting regional-scale subsurface density variation. More detailed and quantitative work utilizing forward modeling has been done (Ammerlaan, 2023) and will be presented in a separate contribution.

2. Geological Setting

The late Paleozoic-Cenozoic geological evolution in Svalbard is well documented through decades of geological field work (e.g., Olaussen et al., 2024; Steel & Worsley, 1984, and references therein). In addition, onshore and offshore 2D reflection seismic data were acquired (Bælum et al., 2012; Eiken, 1985) and 18 petroleum exploration wells and 10 scientific research wells were drilled since 1961 (Senger et al., 2019). These data, however, are of limited use to identify the subsurface stratigraphy, especially at depths where seismic imaging is insufficient and strata are not penetrated by the boreholes. In this context, density constraints from gravity anomaly data can complement field geology and seismic interpretation.

Here we briefly review the geological history of Svalbard. Access to Mesoproterozoic to Ordovician metamorphic and sedimentary units of the pre-Caledonian basement exposed in northern Svalbard is facilitated by an apparent 5° southward tilt of Svalbard (Figure 4). This southward tilt is thought to have initiated in the Early Cretaceous during the emplacement of the HALIP. It exposes the main structural elements such as fault zones and sedimentary basins that are reviewed in Olaussen et al. (2024). In northern Svalbard, the pre-Caledonian basement

Table 1
Synthesis of Deep Geophysical Studies in and Around Svalbard

Study	ID (Figure 3a)	Data type					Acquisition platform (ground, boat, airplane, satellite...)	Comment
		Grav	Mag	S refr	S refl	EM		
Eldholm et al. (1987)	E87				X		Ship (seismic)	Svalbard continental margin
Skilbrei (1991)		X					Aerial	Depth of magnetic basement northern Barents Sea
Skilbrei (1992)		X					Aerial	Basement structure
Fichler et al. (1997)	F97	X					Satellite	Regional structural mapping
Ritzmann et al. (2002)	R02		X		X		Ship	Crustal structure between the Knipovich Ridge and the Van Mijenfjorden
Breivik et al. (2003)	B03	X			X		Ship, (seismic), satellite (gravity)	Crustal structure south of Svalbard
Ritzmann et al. (2004)	R04		X				Ship	transect from Hovgard Ridge to northwestern Svalbard ° across the continental-ocean transition
Geissler and Jokat (2004)	G04	X			X		Ship (seismic)	Northern Svalbard continental margin
Ljones et al. (2004)	L04				X		Ship	Crustal transect from North Atlantic Knipovich Ridge to Svalbard Margin west of Hornsund
Jokat and Micksch (2004)	J04				X		Ship	Sedimentary structure of the Nansen and Amundsen basins
Breivik et al. (2005)	B05	X			X		Satellite (gravimetry), boat (seismic)	Caledonide development onshore-offshore Svalbard
Engen et al. (2009)	E09				X		Ship	Sediment thickness Nansen basin
Olesen et al. (2010)		X	X				Ground, ship, aerial	Compilation of potential field data from Norway, Svalbard and NCS
Minakov et al. (2012a)	M12a	X		X	X		Ship	Seismic tomography offshore Svalbard, including gravity data
Minakov et al. (2012b)	M12b	X	X		X		Ship	Eastern margin/south-east
Krysinski et al. (2013)	K13		X					transect Knipovich Ridge—Spitsbergen—Barents Sea
Marello et al. (2013)	M13	X	X	X	X		Aerial (magnetic), ship (seismic)	Basement of Barents Sea; compilation of magnetic, gravity and seismic data collected over 50 years
Beka et al. (2015)	B15					X	Ground	Lithospheric structure below Svalbard
Klitzke et al. (2016)	K16	X					Satellite	Barents gravity and thermal model
Beka et al. (2017a, 2017b)	B17					X	Magnetotelluric	fault structure below Brøggerhalvøya, magnetotelluric data
Minakov et al. (2018)	M18		X		X		Ship	dyke emplacement HALIP
Lutz et al. (2018)	L18	X	X		X		Ship (seismic, gravity, magnetics)	Basement of the Eurasia Basin
Lasabuda et al. (2018)	La18				X		Ship	Erosion estimates on basis of Neogene-Quaternary sedimentary units
Selway et al. (2020)	S20					X	Magnetotelluric	Upper mantle beneath Svalbard
Dumais and Brønner (2020)	D20	X	X				Aerial, compared to ground-based GPR	Focus on Austfonna sub-glacial bed topography and ice effect on gravity
Grad and Majorowicz (2020)	G20	X	X				Ground (seismological center)	ocean-continent transition

Table 1
Continued

Study	ID (Figure 3a)	Data type				Acquisition platform (ground, boat, airplane, satellite...)	Comment
		Grav	Mag	S refr	S refl		
Dumais et al. (2021)	D21		X			Aerial	spreading evolution of the Knipovich Ridge
Dumais et al. (2022)	D22	X	X	X		Aerial (magnetics)	Lithospheric structure of the Fram Strait
Smeltor et al. (2024)	S24	X	X			Aerial, compilation of surveys of last 4 decades	focus on north Svalbard margin
<i>selected Arctic and regional studies of relevance for this study</i>							
Gaina et al. (2011) and Saltus et al. (2011)	Not shown on map	X	X			Various	Circum-Arctic Mapping Project (CAMP) magnetics and gravity
Døssing et al. (2013)		X	X			Aerial	HALIP
Døssing et al. (2014)		X	X			Aerial	Amundsen Basin
Urlaub et al. (2009)				X		Ship	Eurasia basin gravity and heatflow data
Gómez Dacal et al. (2023)						Various	North Atlantic opening, Iceland Plume, open source density model
Schaeffer and Lebedev (2013)						Various	SL2013sv Upper mantle S-wave tomography model
Lebedeva-Ivanova et al. (2019)						Various	ArcCrust - Crustal thickness and gravity
Straume et al. (2019)						Various	GlobSed - Total sedimentary thickness
Péron-Pindivic et al. (2017)		X	X	X	X	Various	NAGTEC crustal thickness, depth-to-moho, sedimentary thickness
Klitzke et al. (2015)		X	X	X	X	Various	Sedimentary, crustal and LAB depths

Note. EM includes both MT and TEM data.

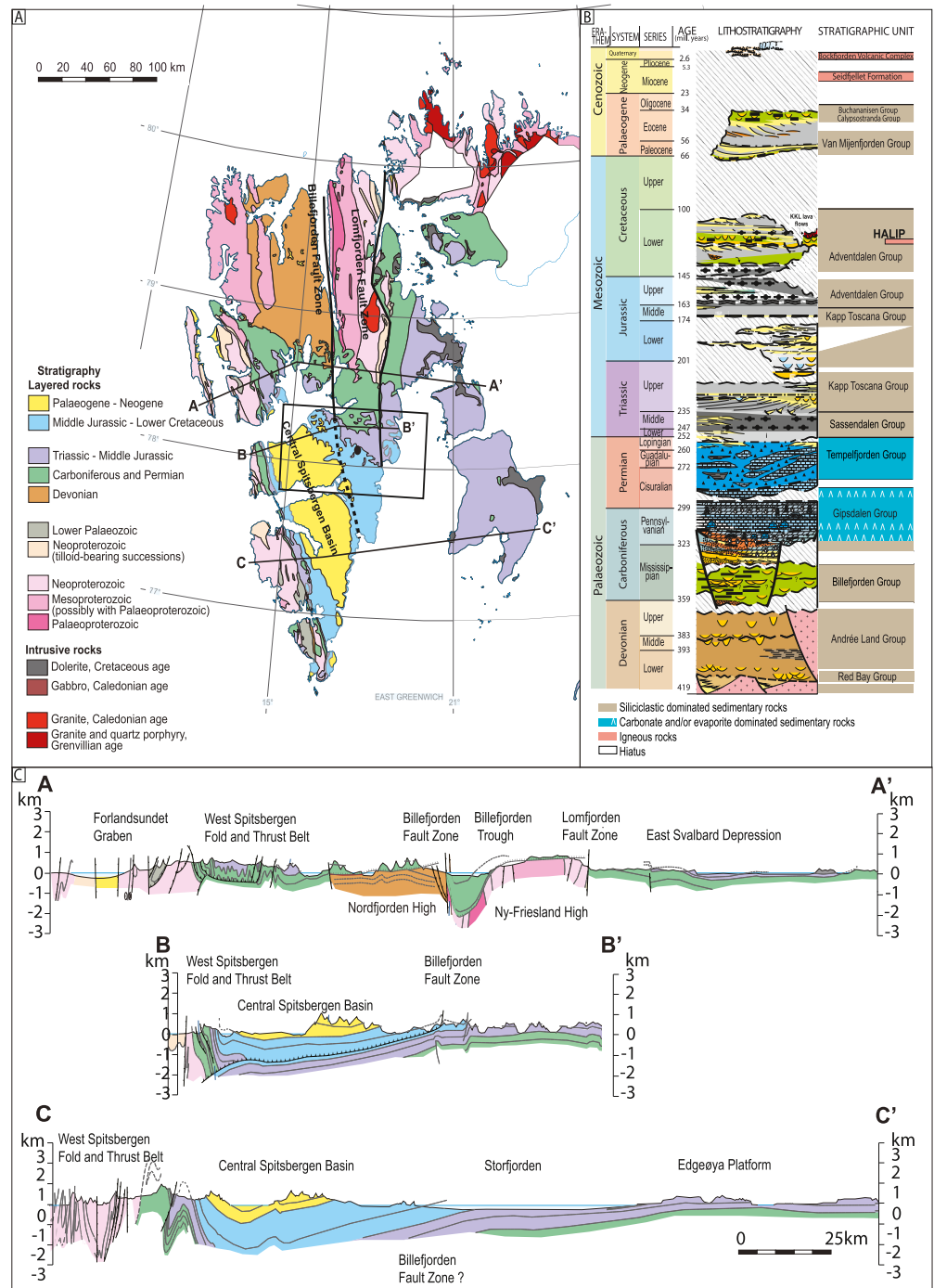


Figure 4. Geological context of the study area. (a) Geological map of Svalbard, illustrating the study area (black rectangle) in a regional context. Locations of cross-sections based largely on surface geological fieldwork and the petroleum exploration borehole at Reindalspasset (black dot) are shown. Map from Dallmann (2015). (b) Devonian-Palaeogene stratigraphic column, introducing the key lithologies and post-Caledonian tectono-stratigraphic evolution. Column adapted from Olaussen et al. (2024). (c) Three regional cross-sections placing the study area in a regional context. Cross-sections adapted from Dallmann (2015).

is segmented by fault-bounded sedimentary basins, including a Devonian collapse basin developed during the collapse of thickened Caledonian crust (e.g., Braathen et al., 2018; Piepjohn, 2000; Séguret et al., 1989) and later by Mid-Late Carboniferous rift basins, such as the Billefjorden Trough (Johannessen & Steel, 1992). These basins

formed along the deep-rooted north-south striking Billefjorden and Lomfjorden fault zones (Figure 4a). Both fault zones show multiphase deformation that initiated in the Upper Paleozoic, followed by major reverse movements and minor strike-slip movements in the Paleogene (Bergh et al., 2011; Braathen et al., 2012; Harland et al., 1974; Piepjohn et al., 2016; Smyrak-Sikora et al., 2021). Southwards, the Upper Paleozoic sedimentary basin fills are draped by Permian carbonate platform units and Mesozoic siliciclastics (Olaussen et al., 2024).

The expression of the Arctic-wide Eureka deformation event is the Paleogene West Spitsbergen Fold and Thrust belt (WSFB, Bergh and Andersen, 1990). In Svalbard, this deformation brings the metamorphic basement to the surface along the west coast of Spitsbergen (Figure 4c). Simultaneously, up to 3,000 m of Permian- Mesozoic sedimentary units (Ishøgda borehole, in Senger et al., 2019) were deformed, and a Paleogene foreland basin, the Central Spitsbergen Basin (previously referred to in the literature as the Central Tertiary Basin), was formed (e.g., Helland-Hansen & Grundvåg, 2021). The Central Spitsbergen Basin was filled with up to 2,000 m of sedimentary siliciclastic units (Figure 4a). The Paleogene contraction also led to reactivation of the deep-rooted Billefjorden and Lomfjorden fault zones (Haremo & Andresen, 1992).

In central Spitsbergen, surface data and seismic surveys allow us to understand the architecture of the Permian to Paleogene subsurface. However, the geological structures underlying the Central Spitsbergen Basin, such as the southward extent of the Devonian collapse basin or the Mid-Late Carboniferous rift basins, are less well understood (Figure 4c). Seismic reflection resolution decreases with depth, limiting the interpretation below the well-illuminated Top Permian unit. The Mid-Late Carboniferous syn-rift units were drilled in the Reindalspasset borehole (Figure 4a), but little is known about the underlying rocks. However, regional trends in gravity data can provide information about crustal-scale structures and top-basement configuration. Gravity data coupled with seismic data can therefore fill the knowledge gap on sub-Permian geological structures.

3. Methods and Data

3.1. Gravity Data Acquisition

The gravity data were acquired in the central Spitsbergen study area (Figure 5) from the 21st of April to 1st of May 2022 using a LaCoste & Romberg gravimeter (Table 2). The instrument still requires a manual gravity measurement deriving the gravity value by classical visual adjustment (Figure 6). It was deployed on the snow surface at single stations arranged along seven profiles (Table 3). The gravity measurements were calibrated at the absolute gravity station “Longyearbyen R” in the basement of the Sysselemesteren house in Longyearbyen (78.223 N, 15.627 E; 982963.796 (mGal) in 2022). The station was originally installed in 1964 and calibrated regularly and was the latest in 2018. For transportation to and from the stations, we used snowmobiles on day trips from Longyearbyen.

The acquisition team involved four persons: one operating the gravimeter, one operating the differential global navigation satellite system (DGNSS) unit, one measuring the snow thickness with an avalanche probe, and one responsible for safety (Figure 6). Each gravity station took approximately 10 min to set up, acquire data and remobilize. The weather conditions during the acquisition campaign were as expected in the high Arctic, with temperatures dropping below -20°C and a moderate breeze (5–8 m/s). When designing the survey, considerations included the avoidance of areas with restricted access to snowmobile traffic and the daily access to the profiles using snowmobiles from the base in Longyearbyen.

3.2. DGNSS: Acquisition and Processing

A Leica Viva GS16 differential global navigation satellite system (DGNSS) receiver (vertical ground offset: 1.80 m) was used in rover mode to acquire the position of the gravimeter. Each point was measured for a duration of at least 3 min. Snow depth was measured using an avalanche probe.

The DGNSS data were processed using the Leica Infinity software package (v. 4.0.0) in post-processing kinematic mode with the $\text{egm08_0N-90N_0E180E_5} \times 5$ geoid model. Stationary base station data were acquired from Statens Kartverket's (the Norwegian Mapping Authority) base station in Longyearbyen (LYRS; TRIMBLE NETR9/5703R51199; TRM41249.00/60111442; located at $78^{\circ} 13' 43.77'' \text{N}$; $15^{\circ} 23' 50.32'' \text{E}$; 495.682 m Ellip. Height). As a quality control of the elevation, the collected data were compared with existing digital elevation model (DEM) data from the Norwegian Polar Institute (2014). These DEM data have a 20 m horizontal resolution. Elevation values for five points with negative elevation values (i.e., values below sea level) in the field

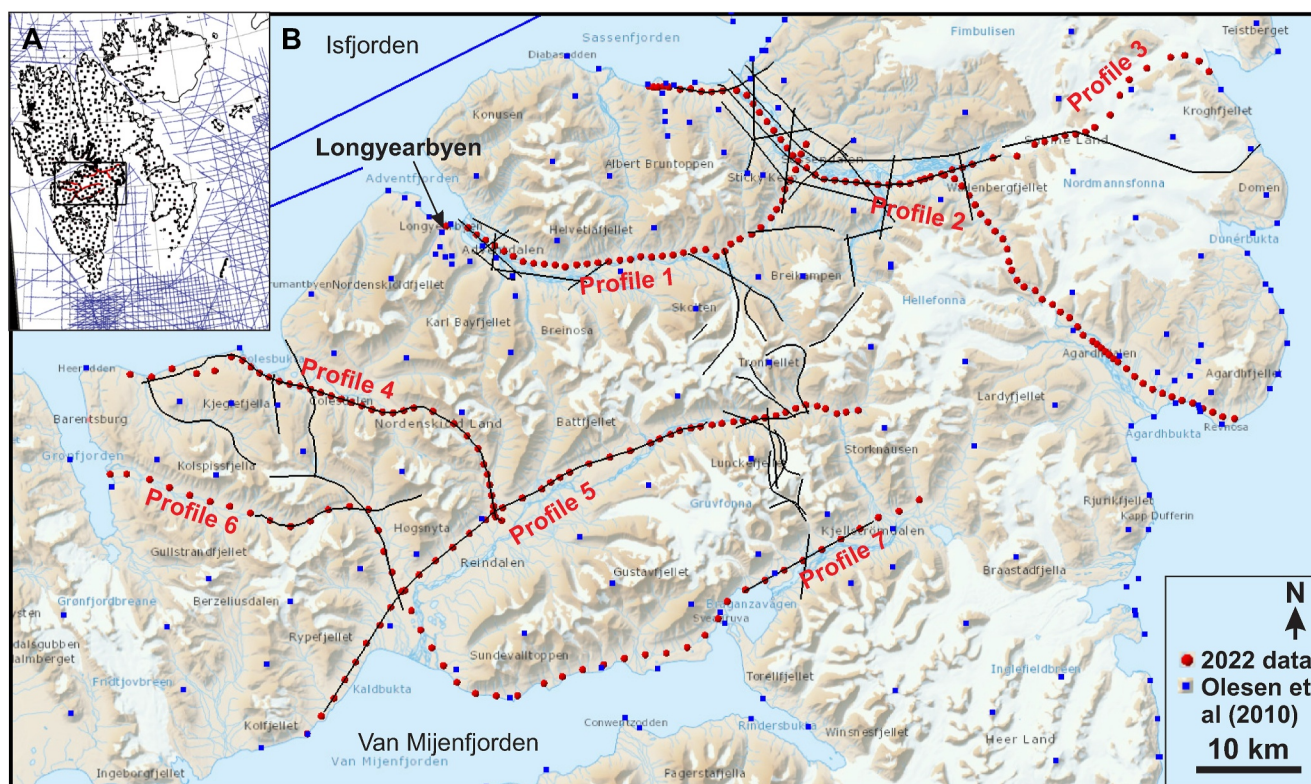


Figure 5. (a) Onshore and offshore land and boat-based gravity data coverage providing data for the regional compilation from Dallmann (2015). (b) Map of acquired gravity stations (red circles) showing also the regional gravity data (blue squares onshore, blue lines in fjords) and the onshore 2D seismic coverage (black lines).

measurements were replaced with the values from the DEM file (i.e., D4.19, D220, D89, D810, D811). The current positioning is considered a significant improvement of the vintage gravity data collected in the late 1980s, but some cm- to dm-scale uncertainty must be expected given the distance to the DGNSS base station in Longyearbyen.

3.3. Gravity Data Processing

We processed the onshore gravity data at the Geological Survey of Norway (NGU) using Seequent Oasis Montaj software. We followed standard processing steps (Saibi, 2018; Figure 7) that incorporate the following corrections (Table 4):

- instrumental drift, which was constrained by two additional measurements at identical locations taken at the start and end of every field day of which tie line intersections provided an estimation of the necessary corrections,

Table 2
Instruments Used in the Acquisition Campaign From 21.4.2022 to 1.5.2022

Instrument	Make	Comment
Gravimeter	Lacoste & Romberg gravimeter	Accuracy of about 0.01 mGal (1 mGal = 10^{-5} m/s ²)
Magnetometer	proton magnetometer from GM Systems Inc.	Acquired while driving, some profiles were not acquired due to technical issues
GPR	Malå ProEx (25 MHz)	For deriving ice thickness on glaciers
DGNSS	Leica Viva GS16	For exact positioning of the gravity stations
Scooter-mounted GPS	Garmin 700	For transit and navigation to gravity sites
Avalanche probe		For measuring snow thickness

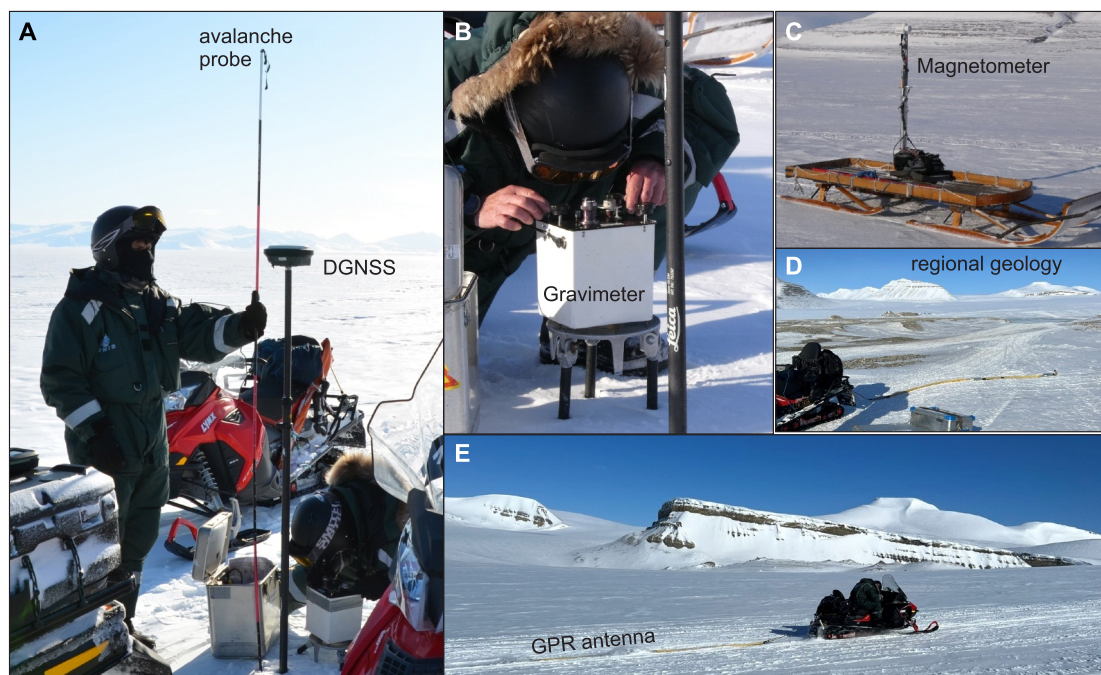


Figure 6. Data acquisition set-up. (a) Positioning of the stations using Leica Viva GS16 dGPS. An avalanche probe is used to measure the snow thickness. (b) The LaCoste & Romberg gravimeter is placed on a tripod during measurements. (c) On several profiles, a magnetometer mounted on a wooden sledge was used. (d) Glacier traverses in eastern Spitsbergen involved acquisition of ground-penetrating radar (GPR) data. (e) GPR data acquisition along Profile 3.

- tidal effects, corrected using the formulas of Longman (1962) implemented in the Oasis Montaj gravity processing module,
- latitude correction was carried out using the Moritz (1980) formula, which led to the World Geodetic System 1984,
- free-air (Li & Götze, 2001),
- Bouguer (using a crustal density of $2,670 \text{ kg/m}^3$ as the widely accepted value for regional gravity studies),
- supplementary terrain correction using combined methods of Kane (1962) and Nagy (1966) as implemented in the Oasis Montaj gravity processing module (also using a crustal density of $2,670 \text{ kg/m}^3$ and a DEM (Norwegian Polar Institute, 2014) for the terrain correction).

This workflow did not include an ice thickness correction, due to the uncertainty of snow and ice depth in 3D. Ground penetrating radar (GPR) measurements obtained along Profile 3, the only glaciated profile, facilitate further correction of the data in the future.

Table 3
Overview of the Acquired Gravity Data Profiles and Corresponding Seismic Lines (Plotted on Figure 9a)

Profile	Location	Length (km)	Number of stations	Seismic line (s)
Profile 1	Adventdalen-Eskerdalen	38.2	39	NH8802-01,-02,-03,-08
Profile 2	Sassendalen-Fulmardalen-Agardhdalen	67.97	74	NH8802-12,-13,-14
Profile 3	Nordmannsfonna	28	20	NH8802-31
Profile 4	Colesdalen	43.65	36	NH9108-02
Profile 5	Reindalen	62.95	44	NH9108-07
				NH8802-32
Profile 6	Grøndalen-Reindalen	49.15	26	NH9108-05,-06
Profile 7	Kjellstrømdalen-Van Mijenfjorden	39.7	21	SVA-VM-85-01, NH8903-21
TOTAL		329.62	260	

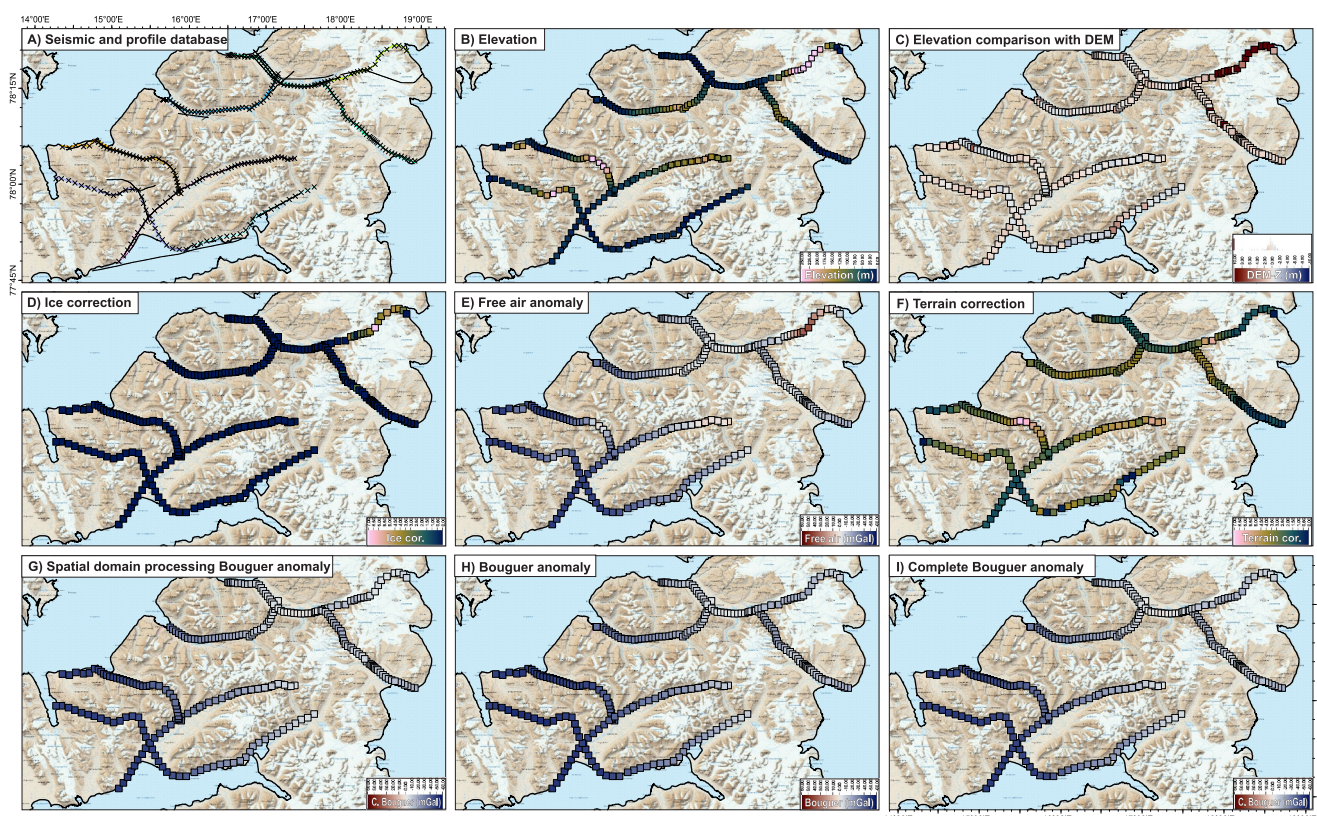


Figure 7. Steps of gravity data processing, including positioning, various corrections and final gravity data, spatially illustrated over the study area. Filled squares correspond to individual station locations (totaling 260) along the seven profiles. (a) Location of the profiles (colored lines), individual stations (black crosses) and available 2D seismic lines (refer to Table 3 for details). (b) Elevation of the gravity points, as measured using the DGNSS system. (c) Quality control of the positioning of the surveys, plotting the elevation difference between the acquired DGNSS data and the regional digital elevation model. The most significant difference occurs across ice caps where ice thickness changes are expected. (d) Ice correction applied in spatial domain gravity processing. (e) Free air anomaly. (f) Terrain correction. (g) Final Bouguer anomaly map from spatial processing. (h) Bouguer anomaly. (i) Complete Bouguer anomaly.

Table 4

Comparison of Processing of the Key Gravity Data Presented in This Study

Data	Data type	Number of stations/ coverage	Comment	Reference(s)
Regional gravity grid	Onshore, aerial and marine gravity data	Onshore: 184 in study area, 1,037 total	Bouguer onshore, free air offshore	Olesen et al. (2010)
Airborne data (SAG98 & SAG99)			Free air only	Forsberg et al. (2002)
Geological maps	Geological maps	All Svalbard	1:100 000	NPI
SVIFT (The Ice-Free Topography of Svalbard)	Sub-Ice-Topography	100 m resolution grid	Does not include radar echo soundings collected alongside gravity data	Fürst et al. (2018)
ArcticDEM - Mosaics, Version 4.1	Surface Topography	10 m resolution		Porter et al. (2023)
International Bathymetric Chart of the Arctic Ocean	Bathymetry	200 m resolution Grid	Upsampled	Jakobsson et al. (2012)

Note. The code for the spatial domain processing is available on GitHub (Liebsch, 2024).

Table 5
Overview of the Data Sets Integrated in This Project

	Vintage data Olesen et al. (2010)	SvalGRAV 2022 processing (this study)	Gravity corrections in spatial domain starting from free air anomaly (this study)
Processing software	Geosoft Oasis Montaj	Geosoft Oasis Montaj	Own code (Liebsch, 2024)
Latitude correction	1980—GRS80 Moritz	1980—GRS80 Moritz	N/A (included in free air anomaly)
Mass correction		Spectral domain, separate Bouguer and terrain correction	Spatial domain: one mass correction
Density used for Bouguer correction	2,670 kg/m ³	2,670 kg/m ³	2,670 kg/m ³ (rock) 917 kg/m ³ (ice)
Used topography data		IBCAO-WGS84 and S0_DTM20 from NPI	ArcticDEM, IBCAO, SVIFT reprojected to 10 m resolution
Ice thickness included?	No	No	Yes
Isostasy correction	Airy isostatic correction: Moho at 30 km depth with a 300 kg/m ³ density contrast	No	No

All results presented in this article are derived from this processing workflow except Figures 7d and 7g derived from the corrections outlined in Section 3.4.

3.4. Gravity Corrections in the Spatial Domain

In addition to the conventional topographic gravity processing outlined in Section 3.3, we compute corrections for topography, ice, and ocean in the spatial domain (Figures 7d and 7g). The workflow starts from the free air anomaly described in 3.3 and the Python code is provided in Liebsch (2024). Modeling gravity in the spatial domain instead of the spectral domain is typically more computationally expensive but also more accurate. To address this, we adopted the approach by Holzrichter et al. (2019), which significantly reduces computational costs while maintaining high accuracy. This method employs high-resolution topography to improve gravity estimates in key areas, while regions that are farther away or smoother, and thus less critical, are modeled at a lower resolution. Instead of using polyhedrons to discretize the topography, as suggested by Holzrichter et al. (2019), we used cuboids and the analytical solution for the gravity volume integral, as presented by Nagy et al. (2000).

To perform the corrections, we compiled a joint DEM from sub-ice topography (SVIFT; Fürst et al., 2018), surface DEM (ArcticDEM; Porter et al., 2023), and bathymetry (IBCAO; Jakobsson et al., 2008; Table 5). Although ice thickness is not well constrained, we used sub-ice topography (SVIFT; Fürst et al., 2018) as an approximation. The merged DEM was resampled to a resolution of 10 m, which is also the highest resolution used for the corrections.

3.5. Magnetic Data: Acquisition

Ground magnetic data were also concurrently acquired along selected profiles (Profiles 1, 2, 3, 7 and the eastern half of Profile 4) whilst driving, with the Overhauser magnetometer from GEM Systems operating continuously from a wooden sledge pulled by a snowmobile (Figure 6c). Data acquisition was continuous at relatively high speeds (ca. 40–50 km/hr). Unfortunately, technical issues with the equipment resulted in an incomplete data set.

3.6. GPR: Acquisition and Processing

Profile 3 crossed a significant ice cap and a GPR unit was used to characterize the ice thickness along the profile. GPR utilizes electromagnetic waves with a fixed radio wavelength to image the shallow subsurface in terms of electric permittivity. GPR is similar to seismic reflection surveying, imaging subsurface boundaries. The electromagnetic waves are emitted radially from the transmitter. Electromagnetic waves that penetrate the subsurface are reflected at interfaces where the electromagnetic properties change and are recorded at the receiver antenna (Robinson et al., 2013).

We used a 25 MHz MALÅ Rough Terrain Antenna (RTA). Data collection was undertaken using a MALÅ ProEx control unit, which handles signal control, timing, sampling, and temporary data storage. On-the-fly data visualization, parameter setup and long-term data storage were handled with the MALÅ XV monitor. Georeferencing of the GPR traces was done with a Garmin eTrex 10 handheld GPS unit, affording m-scale accuracy.

For data acquisition, the RTA setup was hooked up to a snowmobile and dragged while driving at a constant speed of ~ 15 km/hr. We repeatedly crossed the gravimetry profile perpendicular to the gravimetry profile with a line spacing of approximately 10 m. Processing and interpretation of the GPR profiles was undertaken using the ReflexW software (Sandmeier, 2019), following the processing steps outlined by Janocha et al. (2021). The basic processing steps include moving the first arrival to the top of the profile, dewow filtering, energy decay corrections, background removal and time depth conversion. For time-depth conversions, a constant electromagnetic velocity for ice of 0.16 m/ns was used (Robinson et al., 2013). The depth points of the ice thickness were then imported to ArcGIS Pro (version 3.3.1.). Here, we performed a spline function along a narrow swath centered along the profile to extrapolate the glacier thickness along the profile.

3.7. Integration With Other Data

While planning the new gravity survey presented here, and in order to place the new results in a regional context, we integrate geospatial geoscientific data, detailed below and in Table 5.

3.7.1. Regional Gravity Survey

NGU compiled gravity data from various onshore and offshore surveys (Figure 2b; Olesen et al. (2010)). Onshore, the gridded compilation presents Bouguer anomalies, while offshore it shows free air anomalies. The onshore data were largely acquired from 1978 to 1987 by the Norwegian Mapping Authority using both helicopters (for inland sites) and boats (for coastal sites). The mapping campaign came to an end in the summer of 1987 following a fatal helicopter accident on Åsgardfonna in northern Spitsbergen (Statens havarikomisjon, 1989). The compilation also integrates offshore gravity data acquired as part of industry and academic seismic surveys in Svalbard and its surroundings (Figure 3).

The offshore data were acquired along continuous lines, while the onshore data were acquired at stations. Onshore stations were selected to provide semi-regular spacing but also as convenient helicopter landing spots (e.g., tops of peaks and mountains, solid bedrock sites). Typical station spacing is 5–20 km inland and 2–20 km in more accessible coastal sections (Figure 5). The final compilation includes Bouguer corrected data with a density of $2,670 \text{ kg/m}^3$ onshore and free-air data offshore to ensure a continuity between the data sets (Olesen et al., 2010). A standard Moho depth of 30 km with a density contrast of 300 kg/m^3 was applied to estimate the Airy isostatic correction.

3.7.2. Airborne Gravity Data

Airborne gravity has not been systematically acquired over Svalbard (Figure 3b), though aeromagnetic surveys were conducted in the late 1980s–early 1990s (Dallmann, 2015). Additional aerogravity data were acquired during a 1998–1999 campaign using a Twin Otter plane flown out of Longyearbyen (Forsberg & Olesen, 2010; Forsberg et al., 2002). The flight routes were variable. Across Nordaustlandet, where Dumais and Brønner (2020) used the data to characterize the subglacial topography, gravity profiles are oriented along a southwest–northeast (SW–NE) direction with a spacing of 18 km and at a ground clearance of 1 km. Airborne gravity is included in the regional gravity compilation of Olesen et al. (2010).

3.7.3. Non-Gravity Data

To put the gravity data in context, we spatially integrate it with other relevant subsurface data (Table 5). These include magnetic data, petroleum exploration and scientific boreholes onshore Svalbard (Senger et al., 2019), seismic reflection profiles (Bælum et al., 2012; Eiken, 1985), seismic refraction profiles (Ritzmann et al., 2002; Figure 2), regional terrain and bathymetric models (Jakobsson et al., 2008; Norwegian Polar Institute, 2014), non-seismic geophysical profiles (e.g., MT, TEM; Beka et al., 2016, 2017a, 2017b), published maps (e.g., geologic, paleogeographic, tectonic), online map services (e.g., topographic maps, satellite imagery) and digital outcrop

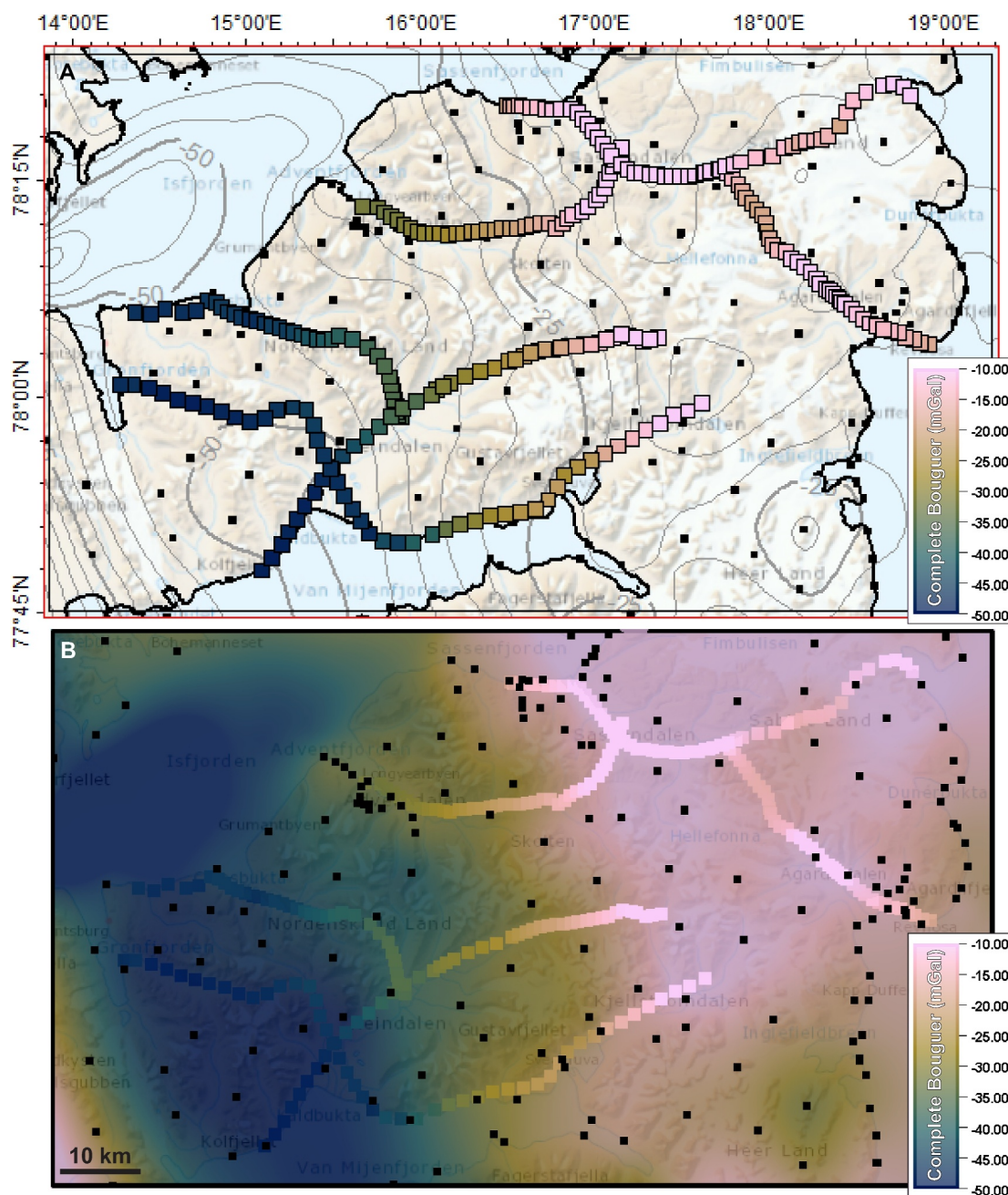


Figure 8. (a) Processed Complete Bouguer anomaly values at the 260 stations from this study (colored squares). The gray contours illustrate the regional gravity grid of Olesen et al. (2010). (b) Onshore gravity data from 2022 overlain with the regional gravity grid of Olesen et al. (2010) for direct comparison. The black squares show the location of the regional gravity stations used by Olesen et al. (2010).

models (e.g., Betlem et al., 2023). All of these are integrated in the Svalbox database in the Petrel software (Senger et al., 2021).

4. Results

4.1. Gravity Data

Figure 8 shows the complete Bouguer anomaly in the final processed gravity data. The recovered values range from -49.4 to -0.3 mGal across the region. The gravity data are consistent with each other where the profiles cross (maximum error of 1.06 mGal) and in the overall trends recorded along individual profiles. Furthermore, the

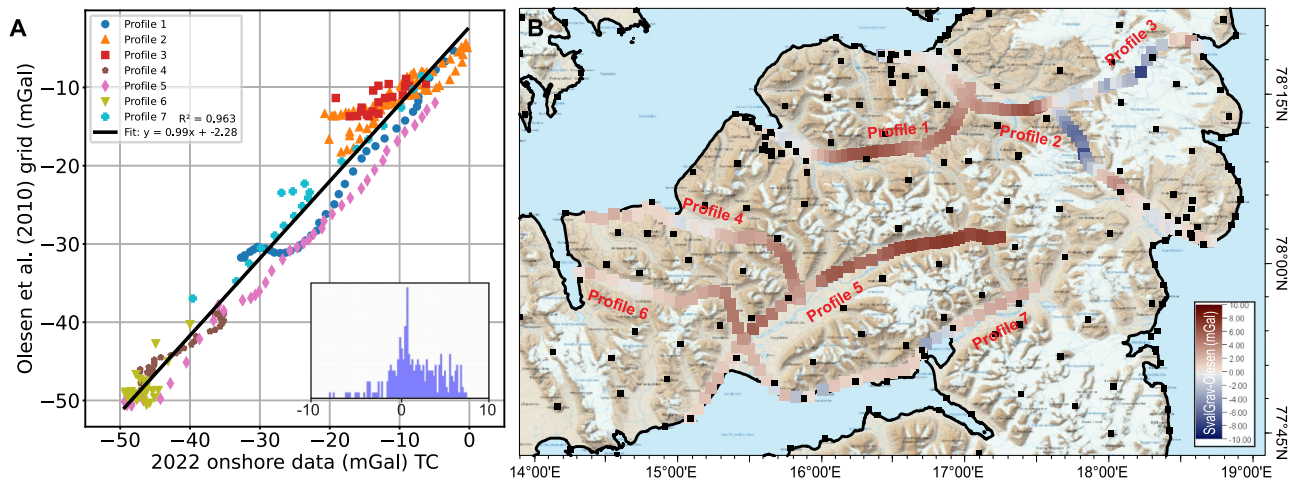


Figure 9. Correlation between the 2022 gravity data and the legacy gridded data from Olesen et al. (2010). (a) Comparison with terrain correction (complete Bouguer anomaly). (b) Spatial comparison of the difference between new (complete Bouguer anomaly) and vintage data. Note that no new terrain correction was applied to the Olesen et al. (2010) data set in this comparison. The difference is calculated as “2022 survey—Olesen et al. (2010).” The location of the gravity points used to generate the vintage gravity grid is illustrated.

new gravity data are consistent with the vintage gravity grid of Olesen et al. (2010) in terms of gravity anomaly trends, as illustrated in Figure 8b. The data show gradual increase by about 50 mGal across 50 km distance toward the east in Profiles 1, 5, and 7 (Figure 8a). Profile 2 crosses a regional high in Sassendalen that is also discernible on the regional gravity grid (Figure 8b). Another smaller positive anomaly is evident in Agardhdalen along the same profile.

4.2. Gravity Data: Comparison of New and Vintage Gravity Data

We compare the new data with the vintage data both statistically (Figure 9a) and spatially (Figure 9b). The difference in the Complete Bouguer anomaly between our new data and the vintage survey is generated by subtracting the vintage values from our survey. Note that the vintage survey (i.e., grid in Olesen et al., 2010) was not acquired at precisely the same locations as our survey presented here, so the comparison is based on a regionally interpolated grid. While the vintage gravity data acquisition focused on the coastal regions and mountaintops easily accessible by helicopter, the 2022 survey presented here largely followed the main valleys where seismic profiles were previously acquired. The topographic position of the points, the gravity effect of the surrounding lithologies in the relatively mountainous study area, slight differences in processing and terrain model used in the processing, all hamper direct comparison. Nonetheless, the data sets still show good agreement with strong correlation (Figure 9a) and consistent trends (Figure 8b). The new data from 2022 will be included when the regional gravity map is being updated by the NGU to the next release of the national gravity database, improving the resolution at the newly sampled locations.

The map also illustrates the station spacing along the individual profiles. The highest priority profile from Longyearbyen to Agardhbukta (Profiles 1 and 2) has a regular station spacing of 1 km. The southernmost profile through Grøndalen, Reindalen and Kjellstrømdalen (Profiles 6 and 7) were acquired with a coarser spacing of 2 km. The middle profiles from Kapp Heer via Colesdalen into Reindalen (Profile 4), and from Van Mijenfjorden to upper Reindalen (Profile 5) had irregular spacings from 1 to 2 km. Spacing was decreased during acquisition in areas where major tectonic lineaments (i.e., Billefjorden Fault Zone) were expected to improve their delineation.

Figure 10 illustrates all seven profiles in the context of the main tectonic elements in the study area (as illustrated in Figure 2). The profiles also compare the 2022 onshore data (points) with the regional grid (black line). Profiles are aligned with the major tectonic elements crossing the study area, including the axis of the Central Spitsbergen Basin and the two major fault zones (Billefjorden and Lomfjorden). In general, there is good agreement between the new and vintage data and the overall trends. The most obvious difference between the vintage and new data is along Profile 3 (where glacier thickness may have changed from the 1980s to 2022) and the central part of Profile 2 (where the new data provide much higher coverage).

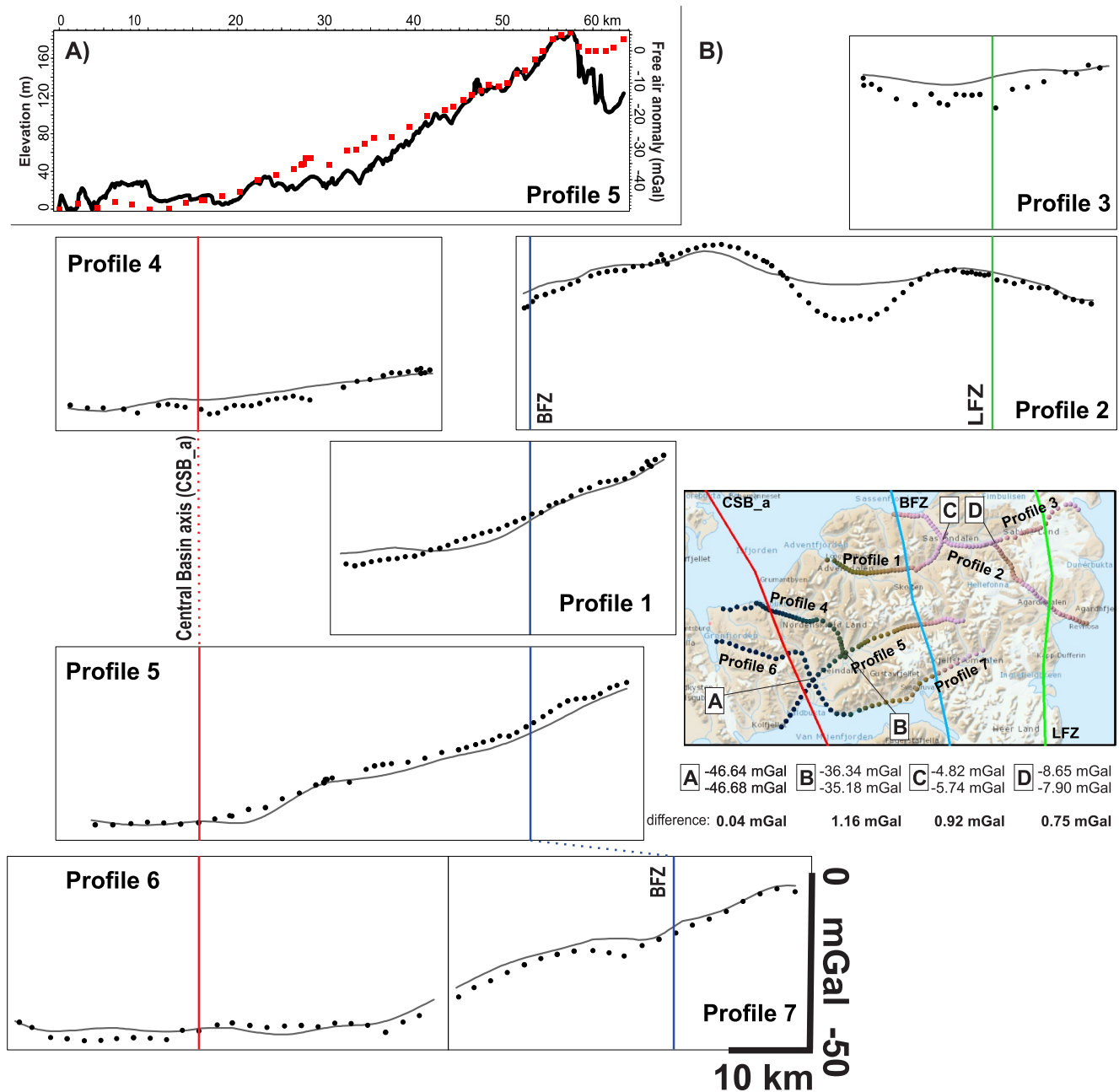


Figure 10. (a) Comparison of the terrain surface and the free air anomaly along Profile 5. (b) Visualization of the recovered gravity anomaly values (in mGal) of all new (2022) gravity data (complete Bouguer anomaly) as station circles along the seven profiles. The intersection with the vertical colored lines is the location of major regional-scale tectonic features including the CSB (Central Spitsbergen Basin—red), BFZ (Billefjorden Fault Zone—blue) and LFZ (Lomfjorden Fault Zone—green). The solid black line corresponding to a profile extracted from the regional gravity grid from Olesen et al. (2010) is displayed for comparison. All profiles are displayed at exactly the same scale. Points A-D illustrate the gravity anomaly values at the points nearest the four profile crossing points.

4.3. Gravity Data: Interpretation With Seismic

Figure 11 illustrates the gravity data through Reindalen along a composite seismic profile. The seismic profile coincides with gravity Profile 5 and crosses the central axis of the Central Spitsbergen Basin in the south-west. Gravity data are constant in the western part of the profile, coinciding with the base of the sedimentary basin. Toward the east, geological mapping and seismic interpretation reveal thinning of the sedimentary package. The gravity anomaly values increase as the underlying higher density rocks are progressively nearer to the surface. A wedge of unknown age and composition is evident below the sediments on the western side of the Billefjorden

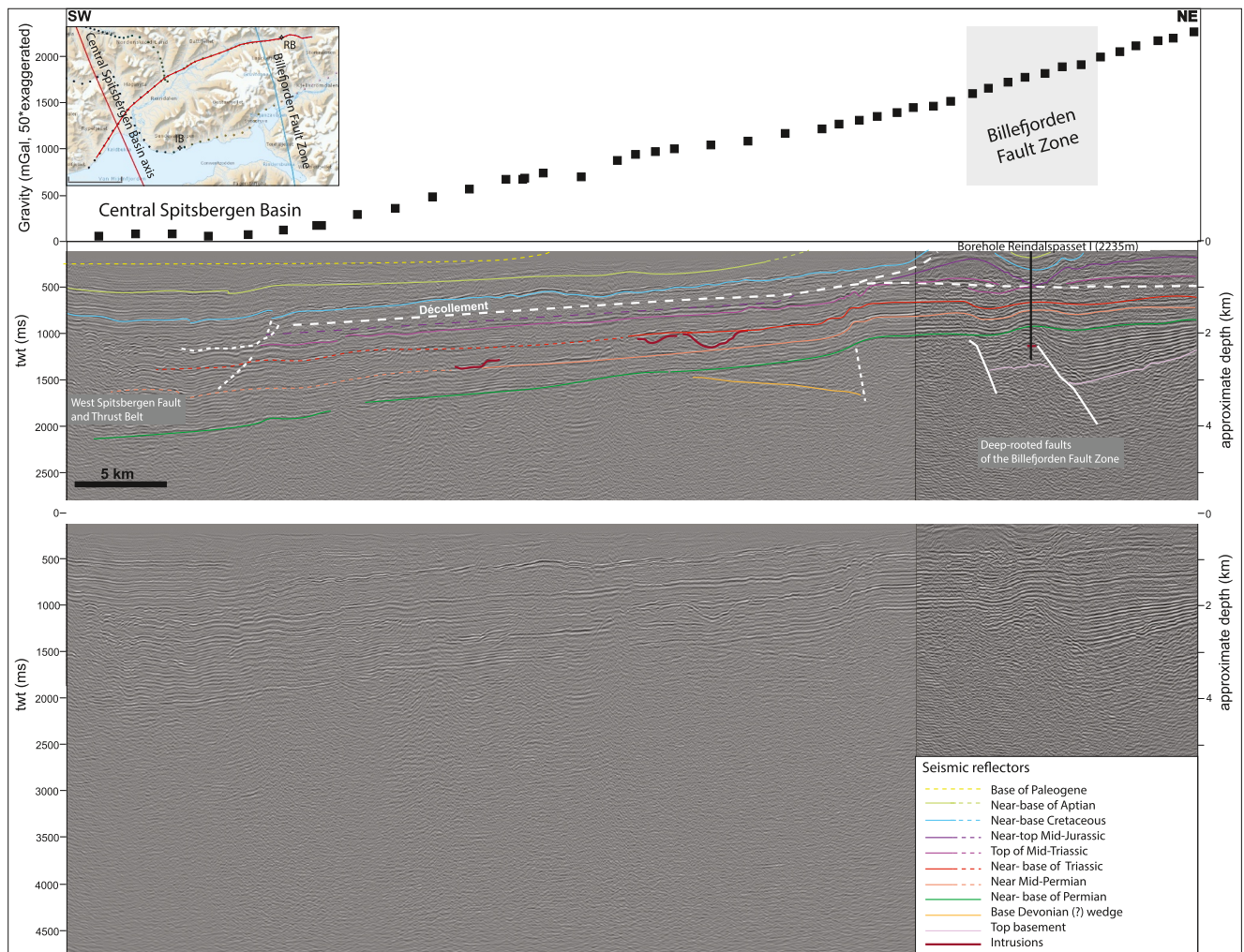


Figure 11. Composite 2D seismic profile directly aligned with Profile 5 through Reindalen. The gravity data are shown with a vertical exaggeration of 50*. The depth scale is in two-way-travel time (twt). The compacted sediments have an average velocity of 4 km/s (Bælum & Braathen, 2012), which was used to calculate an approximate depth scale. IB: Ishøgda Borehole, RB: Reindalspasset borehole.

Fault Zone (Figure 11). The fault zone itself comprises at least two east-dipping fault segments. Syn-rift sediments are visible on the east of the fault zone where seismic reflections define a thickening of the sedimentary package toward the fault zone. These correspond to the middle Carboniferous Billefjorden Trough exposed at the surface ca. 70 km to the north of the profile location. The syn-rift strata are presumably underlain by a thin, partly coal-bearing, pre-rift package and metamorphic basement.

4.4. GPR Results

The gravity signal comprises the entire subsurface, including the effect of snow and ice on the surface. As such, it is crucial to obtain accurate glacier thickness maps for interpreting gravity data. High resolution and up-to-date glacial thickness measurements of the Nordmannsfunna and Königsbergbreen glaciers do not exist. One way of acquiring precise depth measurements is to use GPR (e.g., Fischer, 2009; Hagen & Sætrang, 1991). Our GPR survey along Profile 3 provides high-quality radargrams of the glacier. In Figures 12a and 12b GPR Line 351 is shown as a sample of the GPR survey. Our GPR survey revealed that the glacier has a maximum thickness of 200 m on the highest point of Profile 3. The average glacier thickness is 95 m, thinning at both ends. The areas closest to the end-moraines in the east and west show ice thickness as thin as 4 m (Figure 12c).

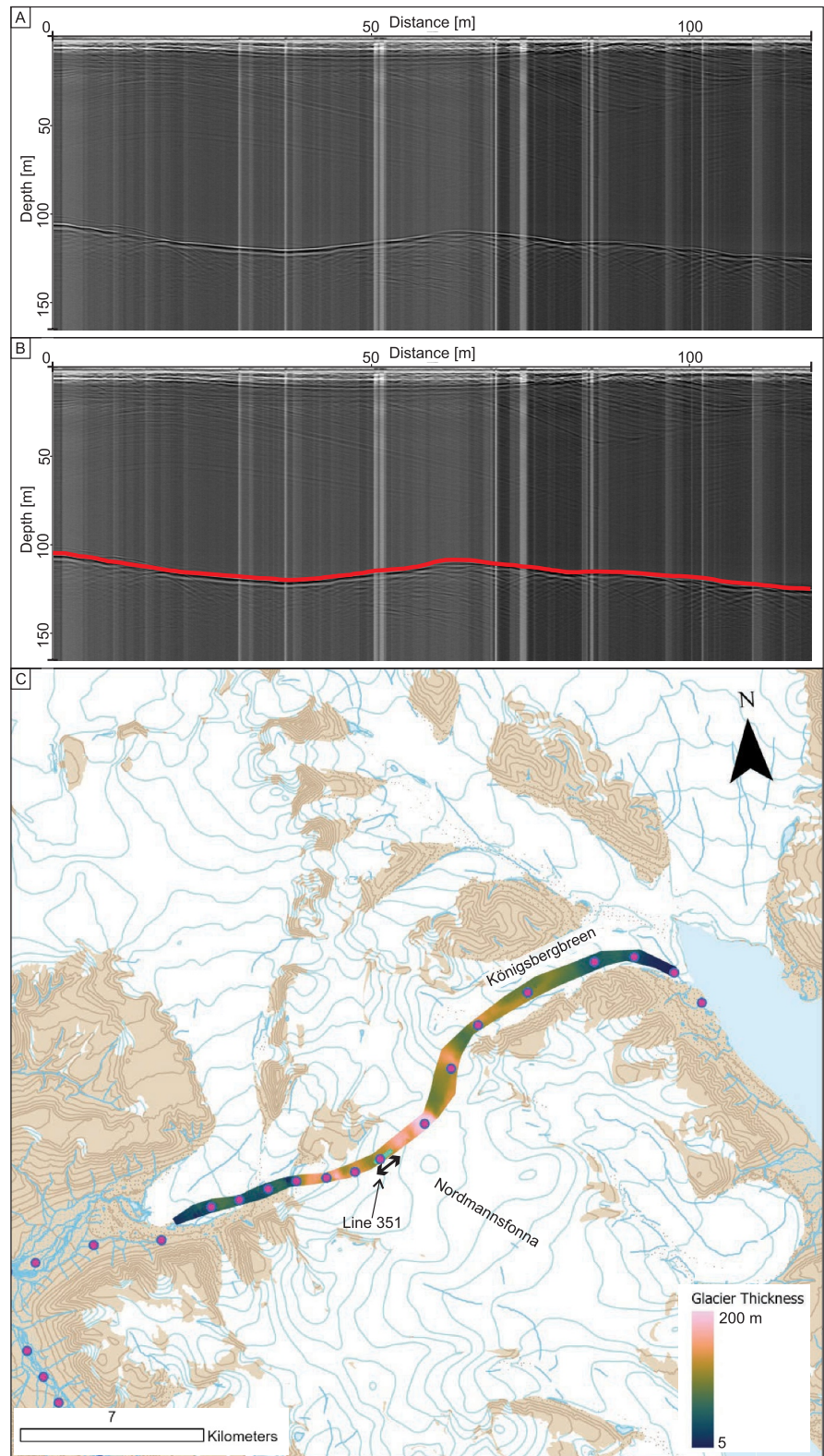


Figure 12. Ground penetrating radar (GPR) survey across the glaciated part of Profile 3 from Sassendalen to Mohnbukta across Nordmannsfunna and Koenigsbergbreen. (a) Sample GPR profile (GPR Line 351), illustrating the processed GPR data. (b) Interpretation of GPR profile, with the top of the bedrock (i.e., base glacier) marked in red. (c) Map of ice thickness along the profile.

5. Discussion

5.1. Synthesis of Deep Geophysical Studies in and Near Svalbard

An overview of existing crustal-scale studies onshore Svalbard and its immediate surroundings are provided in Figure 3 and Table 1. It is convenient to compile this information generally but also in the context of our new gravity data and interpretations. It is worth reiterating that any given geophysical technique is prone to data acquisition variability, non-unique modeling, and interpretation. In this context, the integration of all available data sensing the subsurface with a range of properties (e.g., density, magnetic susceptibility, velocity, resistivity) is crucial.

Existing data and interpretations of regional non-seismic methods include magnetotelluric surveys (Beka et al., 2016, 2017a; Selway et al., 2020), time-domain electromagnetic surveys (Beka et al., 2017b), and gravity modeling along seismic refraction profiles (Breivik et al., 2003). Recent Miocene and Quaternary volcanism suggest a relatively thin lithosphere in NW Spitsbergen based on analyses of mantle xenoliths (e.g., Amundsen et al., 1987). This is of importance given the constraints that the regional lithospheric structure provides on glacial isostatic adjustment modeling (e.g., Auriac et al., 2016). Kierulf et al. (2022) document ongoing uplift in Svalbard using GNSS stations. In Ny-Ålesund, uplift is 9.5 mm/year.

It is worth expanding a little on seismic studies, in particular, as a large number of seismic reflection lines were acquired onshore in the main valleys and in the fjords around Svalbard. This occurred largely during the late 1980s and early 1990s as part of ongoing petroleum exploration (Eiken, 1985). In the 2000s, the Svalex research campaigns systematically acquired seismic profiles in the fjords of western Spitsbergen. Several lines were acquired for characterizing a CO₂ sequestration site in Adventdalen (Bælum et al., 2012). The seismic reflection data, in particular when used for integrating onshore geology, are a powerful tool to constrain fault zone architecture (e.g., Bælum & Braathen, 2012). However, the high sediment velocities (>4 km/s on average), hard seabed reflector offshore, and the presence of onland permafrost with heterogeneous acoustic parameters complicates imaging. Other techniques are therefore required to constrain the deeper part of the subsurface.

5.2. Regional Implications and Interpretation of New Gravity Data

Our new gravity survey covers a region of Svalbard approximately 110 km by 60 km large. It corresponds to an area that is dominated by long-lived north-south trending structural elements, including the Billefjorden and Lomfjorden fault zones and also Devonian, Late Carboniferous and Paleogene basins. We here discuss the recovered signals by integrating our results with vintage gravity data, 2D seismic profiles (Figure 11) and complementary data such as published cross-sections and deep geophysical surveys (Figure 13).

Due to the southerly regional dip of Spitsbergen, the investigated strata are exposed toward the north. The regional cross-section approximately 70 km north of the study area illustrated in Figures 4c and 13 places the new gravity data in a regional structural framework. In the west, the study area is dominated by a gravity low spatially corresponding to the Paleogene Central Spitsbergen Basin foreland basin. The underlying Paleozoic and Mesozoic successions were deformed and tilted during the Paleogene transpression. Together with the non-eroded part of the Cenozoic succession, up to 5 km of sediments are present in this area, tilted toward the west (Figure 11). The Ishøgda exploration borehole located along Profile 6 penetrates 3.3 km of Paleocene-Lower Permian sediments. The Central Spitsbergen Basin along with the post-Caledonian sedimentary succession is underlain by basements of unknown composition and architecture. West of the Billefjorden Fault Zone, the top basement reflector is difficult to interpret on the seismic data (Figure 11). Based on complex top-basement geometries with structural highs and lows seen in surface exposures along northern Spitsbergen (Figure 4), a similarly complex top-basement surface is also expected in sections underlying the Central Spitsbergen Basin. The gravity anomaly data from 2022 present along profile 4 and the western sides of profiles 1, 5, and 6 (Figure 10) show gentle, short-wavelength undulations that might reflect the undulations in top-basement morphology at depth. These undulations are not seen in the regional grid (Olesen et al., 2010; Figure 10) and therefore demonstrate an advantage of using higher-resolution land-based surveys allowing to record details likely originating from top-basement architecture.

The gravity anomaly data consistently increase toward the east from the Central Spitsbergen Basin center, likely reflecting the increased density of the rocks underlying the sedimentary succession and shallower depths to the

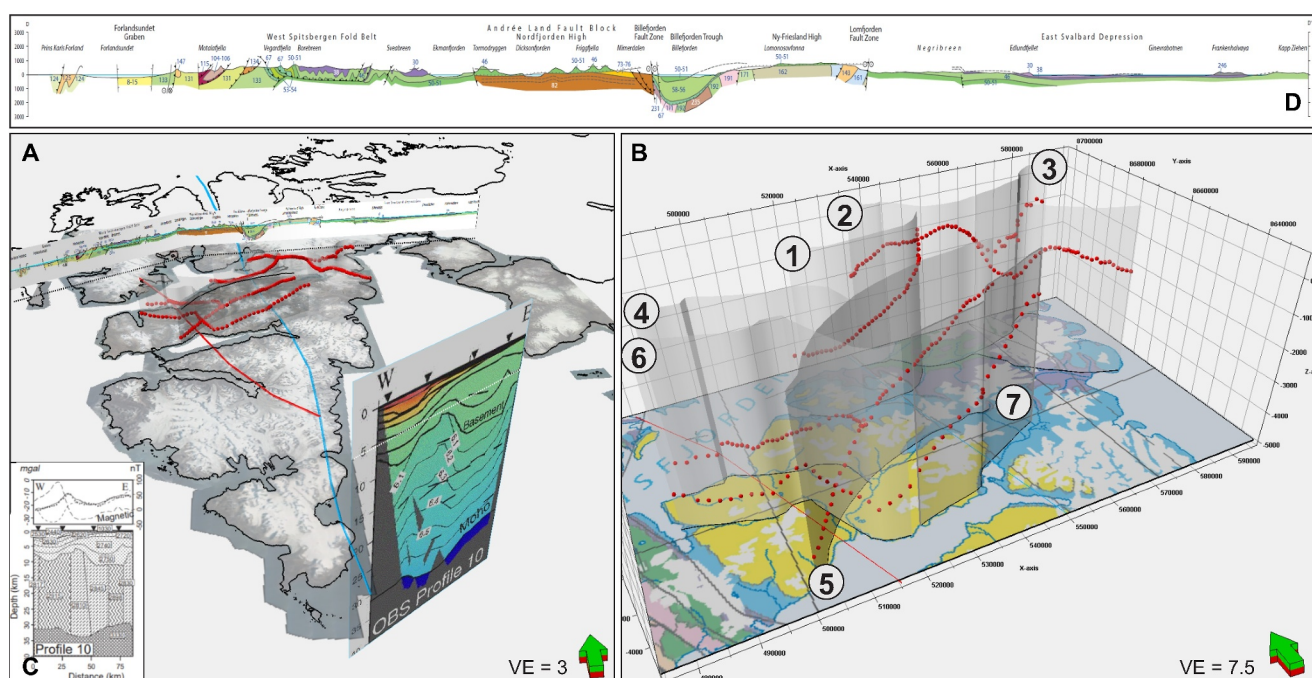


Figure 13. (a) 3D representation of the new gravity data together with a regional geological cross-section (from Dallmann, 2015; Figure 4c) and a deep geophysical profile from Breivik et al. (2005), plotted at 3* vertical exaggeration. The actual gravity data (red points) are plotted with an 80* vertical exaggeration for visualization along the seven profiles. The satellite imagery, coastline, profile locations (dotted lines), axis of Central Spitsbergen Basin (red) and Billefjorden Fault Zone (blue) are all plotted at 5,000 m depth for visualization. Note in particular the lateral basement heterogeneity east of the Billefjorden Fault Zone in both the geological and geophysical cross-sections. (b) Zoom-in of the study area plotted at 7* vertical exaggeration and a geological map plotted at 5,000 m depth for visualization. The black lines at the base of the vertical intersections identify the profile locations. Note the good correlation of individual profiles at crossing points, and the consistent regional trends. (c) Gravity and magnetic data together with a density model of Profile 10 in Breivik et al. (2005). All plotted data are available in the accompanying data package to facilitate different viewing angles. (d) Detailed view of the cross-section from Dallmann 2015 shown in panel A for improved visualization.

top basement (Figures 11 and 13). Similarly, the Paleogene sedimentary package thins toward the north, which is reflected in the increasing gravity values of the northern profiles along the north-south profile (Figures 10 and 13).

Devonian basin fill is exposed to the west of the Billefjorden Fault Zone north of the study area (Figures 4 and 13). It is unclear how far south the Devonian Basin extends, but it may be related to the east-dipping sub-Permian reflection on the Reindalen seismic profile (Figure 11). To the east of the Billefjorden Fault Zone, syn-rift sediments of the Mid-Carboniferous Billefjorden Trough are deposited over a distance of at least 100 km along the fault zone (Figure 13; Bælum & Braathen, 2012). The syn-rift heterogeneous sedimentary units overlie the metamorphic basement. The basement consisting of Mesoproterozoic to Lower Paleozoic units deformed during the Caledonian orogeny is laterally heterogeneous, as illustrated in the cross-section in Figure 13. The Billefjorden Trough is approximately 15 km wide. Surface constraints show that the Billefjorden Fault Zone plunges toward SSE along the eastern flank of the Central Spitsbergen Basin (Figure 4 and blue line in Figure 10, e.g., Bælum & Braathen, 2012). In northern Spitsbergen, the outcropping Billefjorden Fault Zone shows significant deformation, with the metamorphic basement uplifted and faulted over the westward located Devonian basin fill (e.g., eastern flank of the Nordfjorden High, profile A-A' in Figure 4c), related to the Late Devonian Svalbardian event (Bergh et al., 2011; Piepjohn, 2000). The position of the Billefjorden Fault Zone is poorly reflected in the regional gravity data of Olesen et al. (2010; Figure 10). The gravity anomaly data from 2022 expose, however, a sharper inflection along profile 5 (Figure 10) near the location where Billefjorden Fault Zone is expected. The gravity anomaly low seen at profile 7 (Figure 10) is located c. 5 km west of the mapped position of the Billefjorden Fault Zone might indicate significant top-basement topography that could be related to incorrect southward mapping of the Billefjorden Fault Zone. Alternatively, this low gravity anomaly value illustrates the presence of another fault system with an associated thickened sedimentary package toward the west. Such a fault system is, however, not seen in surface geological data.

The Ny Friesland High basement block is sandwiched between the Billefjorden and Lomfjorden fault zones north of the study area (Figure 13). Spatially, it corresponds well to a prominent N-S oriented gravity anomaly. The gravity anomaly is positive in the western part, and negative in the eastern part. Only two profiles cross the Lomfjorden Fault Zone, Profile 2 and Profile 3 (Figure 10). For Profile 2, the short profile length, large station spacing and glacier cover do not allow a picture as clear as Profile 3. Nonetheless, there is a marked decrease in gravity toward the east at the mapped Lomfjorden Fault Zone, possibly indicating syn-rift sediments within the Billefjorden Trough.

To the south of the study area, the N-S gravity anomaly extends into Storfjorden. An ocean bottom seismic refraction profile (Profile 10 in Breivik et al. (2005)), combined with gravity and magnetic data, was used to constrain the density, magnetic susceptibility and velocity structure of the uppermost 40 km. The Moho is located at approximately 30 km depth, with a strongly laterally varying basement structure from 30 to ca. 10 km depth (Figure 13). This lateral heterogeneity is what primarily controls the gravity signal, which is fairly consistent with the profiles in the study area. The uppermost 5–10 km are dominated by more horizontal packages of variable thickness, presumably representing sedimentary units overlying the basement.

In summary, the new gravity data are placed in context by linking onshore geology to the north with deeper seismic refraction profiles to the south.

6. Conclusions

We have acquired new gravity data onshore Svalbard and compared them with vintage regional data. We acquired the new data in April 2022 at 260 individual stations arranged along seven profiles with a cumulative length of 346 km. The survey directly follows 2D seismic profiles to facilitate joint interpretation. We conclude that:

- The new gravity data are consistent with regional gravity data but provide enhanced resolution due to the short station spacing (1–2 km)
- Data indicate a low broad density in the western part of the survey area, dominated by a Cenozoic foreland basin
- A density high occurs in the eastern part of the survey area, narrowing toward the south, likely related to a basement structure
- We co-visualize the gravity data with seismic data along Reindalen, facilitating seismic interpretation at depth
- We place the gravity response in the context of regional geological understanding, particularly the laterally heterogeneous basement in the north and south as determined from outcrops and seismic refraction profiles, respectively

Data Availability Statement

We provide the new gravity, GPR and positioning data in an online and open repository for unrestricted use (Senger and SvalGRAV project team 2024).

References

- Ammerlaan, F. (2023). *Gravity and magnetic data integration for forward modeling in Svalbard* (MSc thesis). University of Utrecht. Retrieved from <https://studenttheses.uu.nl/handle/20.500.12932/45780>
- Amundsen, H., Griffin, W., & O'reilly, S. Y. (1987). The lower crust and upper mantle beneath northwestern Spitsbergen: Evidence from xenoliths and geophysics. *Tectonophysics*, 139(3–4), 169–185. [https://doi.org/10.1016/0040-1951\(87\)90095-3](https://doi.org/10.1016/0040-1951(87)90095-3)
- Auriac, A., Whitehouse, P. L., Bentley, M. J., Patton, H., Lloyd, J. M., & Hubbard, A. (2016). Glacial isostatic adjustment associated with the Barents Sea ice sheet: A modelling inter-comparison. *Quaternary Science Reviews*, 147, 122–135. <https://doi.org/10.1016/j.quascirev.2016.02.011>
- Bagherbandi, M., Amin, H., Wang, L., & Shirazian, M. (2022). Mantle viscosity derived from geoid and different land uplift data in Greenland. *Journal of Geophysical Research: Solid Earth*, 127(8), e2021JB023351. <https://doi.org/10.1029/2021JB023351>
- Bælum, K., & Braathen, A. (2012). Along-strike changes in fault array and rift basin geometry of the Carboniferous Billefjorden Trough, Svalbard, Norway. *Tectonophysics*, 546–547, 38–55. <https://doi.org/10.1016/j.tecto.2012.04.009>
- Bælum, K., Johansen, T. A., Johnsen, H., Rød, K., Ruud, B. O., & Braathen, A. (2012). Subsurface geometries of the Longyearbyen CO2 lab in Central Spitsbergen, as mapped by reflection seismic data. *Norwegian Journal of Geology*, 92, 377–389.
- Beka, T. I., Bergh, S. G., Smirnov, M., & Birkelund, Y. (2017). Magnetotelluric signatures of the complex tertiary fold–thrust belt and extensional fault architecture beneath Brøggerhalvøya. *Svalbard. Polar Research*, 36(1), 1409586. <https://doi.org/10.1080/17518369.2017.1409586>
- Beka, T. I., Senger, K., Autio, U. A., Smirnov, M., & Birkelund, Y. (2017b). Integrated electromagnetic data investigation of a Mesozoic CO2 storage target reservoir–cap–rock succession, Svalbard. *Journal of Applied Geophysics*, 136, 417–430. <https://doi.org/10.1016/j.jappgeo.2016.11.021>

Acknowledgments

Gravity data acquisition was financed by DNO Norge AS, two Arctic Field Grant projects to SR and AS from the Svalbard Science Forum of the Research Council of Norway (RCN; 333159 and 333152, respectively), and the Svalbox project (<https://svalbox.no/>) at the University Centre in Svalbard (UNIS). UNIS provided logistical support during the acquisition and UNIS and the Norwegian Geological Survey (NGU) provided significant in-kind support in data processing and interpretation. GPR data acquisition by JJ was partly supported by the RCN through the Norwegian Research School on Dynamics and Evolution of Earth and Planets (249040/F60). Additional processing, data integration and interpretation was partly conducted as part of the AG351/851 Arctic Tectonics and Volcanism course at UNIS (Senger et al., 2024) financed largely through the NOR-R-AM2 project funded by the RCN (309477). We appreciate the Governor of Svalbard for facilitating data acquisition in the inner part of Reindalen by providing a dispensation for snowmobile travel in a normally restricted area. Schlumberger, Cegal and Seequent generously provided academic licenses for Petrel, Blueback toolbox and Oasis Montaj, respectively. Finally, we sincerely appreciate the constructive comments from Graeme Eagles and an anonymous reviewer, and the editorial handling by Associate Editor Marie-Claude Williamson.

- Beka, T. I., Smirnov, M., Bergh, S. G., & Birkelund, Y. (2015). The first magnetotelluric image of the lithospheric-scale geological architecture in central Svalbard, Arctic Norway. *Polar Research*, 34(1), 26766. <https://doi.org/10.3402/polar.v34.26766>
- Beka, T. I., Smirnov, M., Birkelund, Y., Senger, K., & Bergh, S. G. (2016). Analysis and 3D inversion of magnetotelluric crooked profile data from central Svalbard for geothermal application. *Tectonophysics*, 686, 98–115. <https://doi.org/10.1016/j.tecto.2016.07.024>
- Bergh, S., Maher, H., & Braathen, A. (2011). Late Devonian transpressional tectonics in Spitsbergen, Svalbard, and implications for basement uplift of the Sørkapp–Hornsund High. *Journal of the Geological Society*, 168(2), 441–456. <https://doi.org/10.1144/0016-76492010-046>
- Bergh, S. G., & Andresen, A. (1990). Structural development of the Tertiary fold-and-thrust belt in east Oscar II Land, Spitsbergen. *Polar Research*, 8(2), 217–236. <https://doi.org/10.1111/j.1751-8369.1990.tb00385.x>
- Betlem, P., Rodes, N., Birchall, T., Dahlin, A., Smyrak-Sikora, A., & Senger, K. (2023). The Svalbox digital model database: A geoscientific window to the high Arctic. *Geosphere*, 19(6), 1640–1666. <https://doi.org/10.1130/GES02606.1>
- Braathen, A., Bælum, K., Christiansen, H. H., Dahl, T., Eiken, O., Elvebakk, H., et al. (2012). The Longyearbyen CO₂ Lab of Svalbard, Norway—Initial assessment of the geological conditions for CO₂ sequestration. *Norwegian Journal of Geology*, 353–376.
- Braathen, A., Bergh, S. G., & Maher, H. D., Jr. (1999). Application of a critical wedge taper model to the Tertiary transpressional fold-thrust belt on Spitsbergen. *Svalbard. Geological Society of America Bulletin*, 111(10), 1468–1485. [https://doi.org/10.1130/0016-7606\(1999\)111<1468:AOACWT>2.3.CO;2](https://doi.org/10.1130/0016-7606(1999)111<1468:AOACWT>2.3.CO;2)
- Braathen, A., Osmundsen, P. T., Maher, H., & Ganerød, M. (2018). The Keisarhjelmen detachment records Silurian–Devonian extensional collapse in Northern Svalbard. *Terra Nova*, 30(1), 34–39. <https://doi.org/10.1111/ter.12305>
- Breivik, A. J., Mjelde, R., Grogan, P., Shimamura, H., Murai, Y., & Nishimura, Y. (2003). Crustal structure and transform margin development south of Svalbard based on ocean bottom seismometer data. *Tectonophysics*, 369(1), 37–70. [https://doi.org/10.1016/S0040-1951\(03\)00131-8](https://doi.org/10.1016/S0040-1951(03)00131-8)
- Breivik, A. J., Mjelde, R., Grogan, P., Shimamura, H., Murai, Y., & Nishimura, Y. (2005). Caledonide development offshore–onshore Svalbard based on ocean bottom seismometer, conventional seismic, and potential field data. *Tectonophysics*, 401(1), 79–117. <https://doi.org/10.1016/j.tecto.2005.03.009>
- Crameri, F., Shephard, G. E., & Heron, P. J. (2020). The misuse of colour in science communication. *Nature Communications*, 11(1), 5444. <https://doi.org/10.1038/s41467-020-19160-7>
- Dallmann, W. (2015). Geoscience Atlas of Svalbard. *Norsk Polarinstitutt Rapportserie*, 148, 292p. Retrieved from <http://hdl.handle.net/11250/2580810>
- Døssing, A., Hansen, T. M., Olesen, A. V., Hopper, J. R., & Funck, T. (2014). Gravity inversion predicts the nature of the Amundsen Basin and its continental borderlands near Greenland. *Earth and Planetary Science Letters*, 408, 132–145. <https://doi.org/10.1016/j.epsl.2014.10.011>
- Døssing, A., Jackson, H. R., Matzka, J., Einarsson, I., Rasmussen, T. M., Olesen, A. V., & Brozena, J. M. (2013). On the origin of the Amerasia Basin and the High Arctic Large Igneous Province—Results of new aeromagnetic data. *Earth and Planetary Science Letters*, 363, 219–230. <https://doi.org/10.1016/j.epsl.2012.12.013>
- Dumais, M. A., & Brönnner, M. (2020). Revisiting Austfonna, Svalbard, with potential field methods – A new characterization of the bed topography and its physical properties. *The Cryosphere*, 14(1), 183–197. <https://doi.org/10.5194/tc-14-183-2020>
- Dumais, M.-A., Gernigon, L., Olesen, O., Johansen, S. E., & Brönnner, M. (2021). New interpretation of the spreading evolution of the Knipovich Ridge derived from aeromagnetic data. *Geophysical Journal International*, 224(2), 1422–1428. <https://doi.org/10.1093/gji/ggaa527>
- Dumais, M. A., Gernigon, L., Olesen, O., Lim, A., Johansen, S., & Brönnner, M. (2022). Crustal and thermal heterogeneities across the Fram Strait and the Svalbard margin. *Tectonics*, 41(10), e2022TC007302. <https://doi.org/10.1029/2022TC007302>
- Eiken, O. (1985). Seismic mapping of the post-Caledonian Svalbard. *Polar Research*, 3(2), 167–176. <https://doi.org/10.3402/polar.v3i2.6950>
- Eiken, O. (1994). *Seismic atlas of western Svalbard: A selection of regional seismic transects*. Norsk polarinstitutt Meddelelser #130 (p. 73). Norsk polarinstitutt.
- Eldholm, O., Faleide, J. I., & Myhre, A. M. (1987). Continent-ocean transition at the western Barents Sea/Svalbard continental margin. *Geology*, 15(12), 1118–1122. [https://doi.org/10.1130/0091-7613\(1987\)15<1118:Clatwb>2.0.Co;2](https://doi.org/10.1130/0091-7613(1987)15<1118:Clatwb>2.0.Co;2)
- Engen, Ø., Gjengedal, J. A., Faleide, J. I., Kristoffersen, Y., & Eldholm, O. (2009). Seismic stratigraphy and sediment thickness of the Nansen Basin, Arctic Ocean. *Geophysical Journal International*, 176(3), 805–821. <https://doi.org/10.1111/j.1365-246X.2008.04028.x>
- Faleide, J. I., Tsikalas, F., Breivik, A. J., Mjelde, R., Ritzmann, O., Engen, Ø., et al. (2008). Structure and evolution of the continental margin off Norway and the Barents Sea. *Episodes*, 31(1), 82–91. <https://doi.org/10.18814/epiiugs/2008/v31i1/012>
- Fichler, C., Rundhovde, E., Johansen, S., & Sæther, B. (1997). Barents Sea tectonic structures visualized by ERS1 satellite gravity data with indications of an offshore Baikalian trend. *First Break*, 15(11), 355–363. <https://doi.org/10.1046/j.1365-2397.1997.00678.x>
- Fischer, A. (2009). Calculation of glacier volume from sparse ice-thickness data, applied to Schaufelferner, Austria. *Journal of Glaciology*, 55(191), 453–460. <https://doi.org/10.3189/002214309788816740>
- Forsberg, R., & Olesen, A. V. (2010). Airborne gravity field determination. In G. Xu (Ed.), *Sciences of geodesy - I: Advances and future directions* (pp. 83–104). Springer.
- Forsberg, R., Olesen, A. V., Keller, K., & Møller, M. (2002). Airborne gravity survey of sea areas around Greenland and Svalbard 1999–2001. Survey and processing report. *KMS Technical Report*, 18.
- Fürst, J. J., Navarro, F., Gillet-Chaulet, F., Huss, M., Moholdt, G., Fettweis, X., et al. (2018). The ice-free topography of Svalbard. *Geophysical Research Letters*, 45, 11760–11769. <https://doi.org/10.1029/2018GL079734>
- Gabrielsen, R., Kløvjan, O. S., Haugsbø, H., Midbøe, P. S., Nøttvedt, A., Rasmussen, E., & Skott, P. (1992). A structural outline of Forlandsundet Graben, Prins Karls Forland, Svalbard. *Norsk Geologisk Tidsskrift*, 72, 105–120.
- Gaina, C., Werner, S. C., Saltus, R., & Maus, S., & CAMP GROUP. (2011). Chapter 3 Circum-Arctic mapping project: New magnetic and gravity anomaly maps of the Arctic. *Geological Society, London, Memoirs*, 35(1), 39–48. <https://doi.org/10.1144/m35.3>
- Gee, D. G., Bogolepova, O. K., & Lorenz, H. (2006). The Timanide, Caledonide and Uralide orogens in the Eurasian high Arctic, and relationships to the palaeo-continent Laurentia, Baltica and Siberia. *Geological Society, London, Memoirs*, 32(1), 507–520. <https://doi.org/10.1144/GSL.MEM.2006.032.01.31>
- Geissler, W. H., & Jokat, W. (2004). A geophysical study of the northern Svalbard continental margin. *Geophysical Journal International*, 158(1), 50–66. <https://doi.org/10.1111/j.1365-246X.2004.02315.x>
- Gómez Dacal, M. L., Scheck-Wenderoth, M., Faleide, J. I., Abdelmalak, M. M., Bott, J., & Anikiev, D. (2023). Tracing the Iceland plume and North East Atlantic breakup in the lithosphere. *Communications Earth & Environment*, 4(1), 457. <https://doi.org/10.1038/s43247-023-01120-w>
- Grad, M., & Majorowicz, J. (2020). Geophysical properties of the crust and upper mantle of the ocean-continent transition in Svalbard area. *Polish Polar Research*, 1-22-1–22. <https://doi.org/10.24425/ppr.2020.132567>
- Hagen, J. O., & Sætrang, A. (1991). Radio-echo soundings of sub-polar glaciers with low-frequency radar. *Polar Research*, 9(1), 99–107. <https://doi.org/10.1111/j.1751-8369.1991.tb00405.x>

- Haremo, P., & Andresen, A. (1992). Tertiary décollement thrusting and inversion structures along Billefjorden and Lomfjorden Fault Zones, east central Spitsbergen. In *Structural and tectonic modelling and its application to petroleum geology* (pp. 481–494). Norwegian Petroleum Society Special Publications. <https://doi.org/10.1016/B978-0-444-88607-1.50038-3>
- Harland, W. B., Cutbill, J. L., Friend, P. F., Gobbet, D. J., Holliday, D. W., Maton, P. I., et al. (1974). The Billefjorden Fault Zone, Spitsbergen, the long history of a major tectonic lineament. *Norsk Polarinstittut Skrifter*, 161.
- Helland-Hansen, W., & Grundvåg, S.-A. (2021). The Svalbard Eocene-Oligocene (?) Central Basin succession: Sedimentation patterns and controls. *Basin Research*, 33(1), 729–753. <https://doi.org/10.1111/bre.12492>
- Holzrichter, N., Szwillus, W., & Götze, H.-J. (2019). An adaptive topography correction method of gravity field and gradient measurements by polyhedral bodies. *Geophysical Journal International*, 218(2), 1057–1070. <https://doi.org/10.1093/gji/ggz211>
- Jakobsson, M., Macnab, R., Mayer, L., Anderson, R., Edwards, M., Hatzky, J., et al. (2008). An improved bathymetric portrayal of the Arctic Ocean: Implications for ocean modeling and geological, geophysical and oceanographic analyses. *Geophysical Research Letters*, 35(7), L07602. <https://doi.org/10.1029/2008GL033520>
- Jakobsson, M., Mayer, L., Coakley, B., Dowdeswell, J. A., Forbes, S., Fridman, B., et al. (2012). The International bathymetric Chart of the Arctic Ocean (IBCAO) version 3.0. *Geophysical Research Letters*, 39(12). <https://doi.org/10.1029/2012GL052219>
- Janocha, J., Smyrak-Sikora, A., Senger, K., & Birchall, T. (2021). Seeing beyond the outcrop: Integration of ground-penetrating radar with digital outcrop models of a paleokarst system. *Marine and Petroleum Geology*, 125, 104833. <https://doi.org/10.1016/j.marpetgeo.2020.104833>
- Johannessen, E. P., & Steel, R. J. (1992). Mid-carboniferous extension and rift-infill sequences in the Billefjorden Trough, Svalbard. *Norsk Geologisk Tidsskrift*, 72, 35–48.
- Jokat, W., & Micksch, U. (2004). Sedimentary structure of the Nansen and Amundsen basins, Arctic Ocean. *Geophysical Research Letters*, 31(2). <https://doi.org/10.1029/2003GL018352>
- Kane, M. F. (1962). A comprehensive system of terrain corrections using a digital computer. *Geophysics*, 27(4), 455–462. <https://doi.org/10.1190/1.1439044>
- Kierulf, H. P., Kohler, J., Boy, J.-P., Geyman, E. C., Mémin, A., Omang, O. C., et al. (2022). Time-varying uplift in Svalbard—An effect of glacial changes. *Geophysical Journal International*, 231(3), 1518–1534. <https://doi.org/10.1093/gji/ggac264>
- Klitzke, P., Faleide, J. I., Scheck-Wenderoth, M., & Sippel, J. (2015). A lithosphere-scale structural model of the Barents Sea and Kara Sea region. *Solid Earth*, 6, 153–172. <https://doi.org/10.5194/se-6-153-2015>
- Klitzke, P., Sippel, J., Faleide, J. I., & Scheck-Wenderoth, M. (2016). A 3D gravity and thermal model for the Barents Sea and Kara Sea. *Tectonophysics*, 684, 131–147. <https://doi.org/10.1016/j.tecto.2016.04.033>
- Krysiński, L., Grad, M., Mjelde, R., Czuba, W., & Guterch, A. (2013). Seismic and density structure of the lithosphere–asthenosphere system along transect Knipovich Ridge–Spitsbergen–Barents Sea—geological and petrophysical implications. *Polish Polar Research*, 34(2), 111–138. <https://doi.org/10.2478/popore-2013-0011>
- Lasabuda, A., Geissler, W. H., Laberg, J. S., Knutsen, S.-M., Rydningen, T. A., & Berglar, K. (2018). Late cenozoic erosion estimates for the northern Barents Sea: Quantifying glacial sediment input to the Arctic Ocean. *Geochemistry, Geophysics, Geosystems*, 19(12), 4876–4903. <https://doi.org/10.1029/2018GC007882>
- Lasabuda, A. P. E., Johansen, N. J. S., Laberg, J. S., Faleide, J. I., Senger, K., Rydningen, T. A., et al. (2021). Cenozoic uplift and erosion of the Norwegian Barents Shelf – A review. *Earth-Science Reviews*, 217, 1–35. <https://doi.org/10.1016/j.earscirev.2021.103609>
- Lebedeva-Ivanova, N., Gaina, C., Minakov, A., & Kashubin, S. (2019). ArcCRUST: Arctic crustal thickness from 3-D gravity inversion. *Geochemistry, Geophysics, Geosystems*, 20(7), 3225–3247. <https://doi.org/10.1029/2018GC008098>
- Li, X., & Götze, H.-J. (2001). Ellipsoid, geoid, gravity, geodesy, and geophysics. *Geophysics*, 66(6), 1660–1668. <https://doi.org/10.1190/1.1487109>
- Liebsch, J. (2024). Adaptive-forward-gravity. Processing code. <https://github.com/JonasLiebsch/Adaptive-Forward-Gravity>
- Ljones, F., Kuwano, A., Mjelde, R., Breivik, A., Shimamura, H., Murai, Y., & Nishimura, Y. (2004). Crustal transect from the North Atlantic Knipovich ridge to the Svalbard margin west of Hornsund. *Tectonophysics*, 378(1), 17–41. <https://doi.org/10.1016/j.tecto.2003.10.003>
- Longman, I. M. (1962). A Green's function for determining the deformation of the Earth under surface mass loads: I. Theory. *Journal of Geophysical Research* (1896-1977), 67(2), 845–850. <https://doi.org/10.1029/JZ067i002p00845>
- Lutz, R., Franke, D., Berglar, K., Heyde, I., Schreckenberger, B., Klitzke, P., & Geissler, W. H. (2018). Evidence for mantle exhumation since the early evolution of the slow-spreading Gakkel Ridge, Arctic Ocean. *Journal of Geodynamics*, 118, 154–165. <https://doi.org/10.1016/j.jog.2018.01.014>
- Maher, H. D., Jr. (2001). Manifestations of the Cretaceous High Arctic Large Igneous Province in Svalbard. *The Journal of Geology*, 109(1), 91–104. <https://doi.org/10.1086/317960>
- Marello, L., Ebbing, J., & Gernigon, L. (2013). Basement inhomogeneities and crustal setting in the Barents Sea from a combined 3D gravity and magnetic model. *Geophysical Journal International*, 193(2), 557–584. <https://doi.org/10.1093/gji/ggt018>
- Minakov, A., Faleide, J. I., Glebovsky, V. Y., & Mjelde, R. (2012a). Structure and evolution of the northern Barents–Kara Sea continental margin from integrated analysis of potential fields, bathymetry and sparse seismic data. *Geophysical Journal International*, 188(1), 79–102. <https://doi.org/10.1111/j.1365-246X.2011.05258.x>
- Minakov, A., Mjelde, R., Faleide, J. I., Flueh, E. R., Dannowski, A., & Keers, H. (2012b). Mafic intrusions east of Svalbard imaged by active-source seismic tomography. *Tectonophysics*, 518–521, 106–118. <https://doi.org/10.1016/j.tecto.2011.11.015>
- Minakov, A., Yarushina, V., Faleide, J. I., Krupnova, N., Sakoulina, T., Dergunov, N., & Glebovsky, V. (2018). Dyke emplacement and crustal structure within a continental large igneous province, northern Barents Sea. *Geological Society, London, Special Publications*, 460(1), 371–395. <https://doi.org/10.1144/SP460.4>
- Moritz, H. (1980). Geodetic reference system 1980. *Bulletin Geodesique*, 54(3), 395–405. <https://doi.org/10.1007/BF02521480>
- Müller, R. D., Zahirovic, S., Williams, S. E., Cannon, J., Seton, M., Bower, D. J., et al. (2019). A global plate model including lithospheric deformation along major rifts and orogens since the Triassic. *Tectonics*, 38(6), 1884–1907. <https://doi.org/10.1029/2018TC005462>
- Muto, A., Christianson, K., Horgan, H. J., Anandakrishnan, S., & Alley, R. B. (2013). Bathymetry and geological structures beneath the Ross Ice Shelf at the mouth of Whillans Ice Stream, West Antarctica, modeled from ground-based gravity measurements. *Journal of Geophysical Research: Solid Earth*, 118(8), 4535–4546. <https://doi.org/10.1002/jgrb.50315>
- Nagy, D. (1966). The gravitational attraction of a right rectangular prism. *Geophysics*, 31(2), 362–371. <https://doi.org/10.1190/1.1439779>
- Nagy, D., Papp, G., & Benedek, J. (2000). The gravitational potential and its derivatives for the prism. *Journal of Geodesy*, 74(7), 552–560. <https://doi.org/10.1007/s001900000116>
- Norwegian Polar Institute. (2014). Geological and topographic data from Svalbard: Geodata.npolar.no.

- Nøttvedt, A., Livbjerg, F., Midbøe, P. S., & Rasmussen, E. (1993). Hydrocarbon potential of the Central Spitsbergen Basin. In T. O. Vorren, E. Bergsager, Ø. A. Dahl-Stammes, E. Holter, B. Johansen, E. Lie, et al. (Eds.), *Arctic geology and petroleum potential* (pp. 333–361). Elsevier.
- Olaussen, S., Grundvåg, S.-A., Senger, K., Anell, I., Betlem, P., Birchall, T., et al. (2024). Svalbard composite tectono-sedimentary element, Barents Sea. *Geological Society, London, Memoirs*, 57(1), M57-2021-36. <https://doi.org/10.1144/M57-2021-36>
- Olesen, O., Brønner, M., Ebbing, J., Gellein, J., Gemignon, L., Koziel, J., et al. (2010). New aeromagnetic and gravity compilations from Norway and adjacent areas: Methods and applications. *Geological Society, London, Petroleum Geology Conference series*, 7(1), 559–586. <https://doi.org/10.1144/0070559>
- Pease, V., Drachev, S., Stephenson, R., & Zhang, X. (2014). Arctic lithosphere — A review. *Tectonophysics*, 628, 1–25. <https://doi.org/10.1016/j.tecto.2014.05.033>
- Péron-Pinvidic, G., Hopper, J. R., Stoker, M., Gaina, C., Funck, T., Árting, U. E., & Doornenbal, J. C. (2017). The NE Atlantic region: A reappraisal of crustal structure, tectonostratigraphy and magmatic evolution—an introduction to the NAG-TEC project. *Geological Society, London, Special Publications*, 447(1), 1–10. <https://doi.org/10.1144/SP447.17>
- Petrov, O., Morozov, A., Shokalsky, S., Kashubin, S., Artemieva, I. M., Sobolev, N., et al. (2016). Crustal structure and tectonic model of the Arctic region. *Earth-Science Reviews*, 154, 29–71. <https://doi.org/10.1016/j.earscirev.2015.11.013>
- Piepjoh, K. (2000). The Svalbardian-Ellesmerian deformation of the Old Red Sandstone and the pre-Devonian basement in NW Spitsbergen (Svalbard). *Geological Society, London, Special Publications*, 180(1), 585–601. <https://doi.org/10.1144/gsl.sp.2000.180.01.31>
- Piepjoh, K., von Gosen, W., & Tessensohn, F. (2016). The Eureka deformation in the Arctic: An outline. *Journal of the Geological Society*, 173(6), 1007–1024. <https://doi.org/10.1144/jgs2016-081>
- Porter, C., Howat, I., Noh, M.-J., Husby, E., Khuvis, S., Danish, E., et al. (2023). ArcticDEM - Mosaics, version 4.1 [dataset] Polar Geospatial Centre. ArcticDEM. Harvard Dataverse. <https://doi.org/10.7910/DVN/3VDC4W>
- Ritzmann, O., Jokat, W., Czuba, W., Guterch, A., Mjelde, R., & Nishimura, Y. (2004). A deep seismic transect from Hovgård Ridge to north-western Svalbard across the continental-ocean transition: A sheared margin study. *Geophysical Journal International*, 157(2), 683–702. <https://doi.org/10.1111/j.1365-246X.2004.02204.x>
- Ritzmann, O., Jokat, W., Mjelde, R., & Shimamura, H. (2002). Crustal structure between the Knipovich Ridge and the Van Mijenfjorden (Svalbard). *Marine Geophysical Researches*, 23(5–6), 379–401. <https://doi.org/10.1023/B:MARI.0000018168.89762.a4>
- Robinson, M., Bristow, C., McKinley, J., & Ruffell, A. (2013). 1.5. 5. Ground penetrating radar. *Geomorphological techniques*.
- Saibi, H. (2018). Microgravity and its applications in geosciences. In *Gravity book* (Intech edition, pp. 41–72).
- Saltus, R. W., Miller, E. L., Gaina, C., & Brown, P. J. (2011). Chapter 4 Regional magnetic domains of the Circum-Arctic: A framework for geodynamic interpretation. *Geological Society, London, Memoirs*, 35(1), 49–60. <https://doi.org/10.1144/m35.4>
- Sandmeier, K. (2019). ReflexW-GPR and seismic processing software [software]. Sandmeier. <https://www.sandmeier-geo.de/reflexw.html>
- Schaaf, N. W., Osmundsen, P. T., Van der Lelij, R., Schönenberger, J. L., Lenz, O. K., Redfield, T., & Senger, K. (2021). Tectono-sedimentary evolution of the eastern Forlandsundet Graben, Svalbard. *Norwegian Journal of Geology*, 100. <https://doi.org/10.1785/njg100-4-4>
- Schaeffer, A. J., & Lebedev, S. (2013). Global shear speed structure of the upper mantle and transition zone. *Geophysical Journal International*, 194(1), 417–449. <https://doi.org/10.1093/gji/ggt095>
- Séguret, M., Séranne, M., Chauvet, A., & Brunel, A. (1989). Collapse basin: A new type of extensional sedimentary basin from the Devonian of Norway. *Geology*, 17(2), 127–130. [https://doi.org/10.1130/0091-7613\(1989\)017<0127:cbant>2.3.co;2](https://doi.org/10.1130/0091-7613(1989)017<0127:cbant>2.3.co;2)
- Selway, K., Smirnov, M. Y., Beka, T., O'Donnell, J. P., Minakov, A., Senger, K., et al. (2020). Magnetotelluric constraints on the temperature, composition, partial melt content, and viscosity of the upper mantle beneath Svalbard. *Geochemistry, Geophysics, Geosystems*, 21(5), e2020GC008985. <https://doi.org/10.1029/2020GC008985>
- Senger, K., & SvalGRAV project team. (2024). Crustal heterogeneity onshore central Spitsbergen: Insights from new gravity and vintage geophysical data (digital appendix) [Dataset]. Zenodo. <https://doi.org/10.5281/zenodo.14187127>
- Senger, K., Betlem, P., Birchall, T., Buckley, S. J., Coakley, B., Eide, C. H., et al. (2021). Using digital outcrops to make the high Arctic more accessible through the Svalbox database. *Journal of Geoscience Education*, 69(2), 123–137. <https://doi.org/10.1080/10899995.2020.1813865>
- Senger, K., Brugmans, P., Grundvåg, S.-A., Jochmann, M., Nøttvedt, A., Olaussen, S., et al. (2019). Petroleum exploration and research drilling onshore Svalbard: A historical perspective. *Norwegian Journal of Geology*, 99(3), 1–30. <https://doi.org/10.17850/njg99-3-1>
- Senger, K., Nuus, M., Balling, N., Betlem, P., Birchall, T., Christiansen, H. H., et al. (2023). The subsurface thermal state of Svalbard and implications for geothermal potential. *Geothermics*, 111, 102702. <https://doi.org/10.1016/j.geothermics.2023.102702>
- Senger, K., Shephard, G., Ammerlaan, F., Anfinson, O., Audet, P., Coakley, B., et al. (2024). Arctic tectonics and volcanism: A multi-scale, multidisciplinary educational approach. *Geoscience Communication*, 2024, 1–47. <https://doi.org/10.5194/gc-2024-3>
- Senger, K., Tveranger, J., Ogata, K., Braathen, A., & Planke, S. (2014). Late Mesozoic magmatism in Svalbard: A review. *Earth-Science Reviews*, 139, 123–144. <https://doi.org/10.1016/j.earscirev.2014.09.002>
- Skilbrei, J. R. (1991). Interpretation of depth to the magnetic basement in the northern Barents Sea (south of Svalbard). *Tectonophysics*, 200(1–3), 127–141. [https://doi.org/10.1016/0040-1951\(91\)90010-p](https://doi.org/10.1016/0040-1951(91)90010-p)
- Skilbrei, J. R. (1992). Preliminary interpretation of aeromagnetic data from Spitsbergen, Svalbard Archipelago (76°–79°N): Implications for structure of the basement. *Marine Geology*, 106(1–2), 53–68. [https://doi.org/10.1016/0025-3227\(92\)90054-1](https://doi.org/10.1016/0025-3227(92)90054-1)
- Smelror, M., Olaussen, S., Dumais, M.-A., Grundvåg, S.-A., & Abay, T. B. (2024). Northern Svalbard composite tectono-sedimentary element. *Geological Society, London, Memoirs*, 57(1), M57-2023-2. <https://doi.org/10.1144/M57-2023-2>
- Smyrak-Sikora, A., Nicolaisen, J., Braathen, A., Johannessen, E. P., Olaussen, S., & Stemmerik, L. (2021). Impact of growth faults on mixed siliciclastic-carbonate-evaporite deposits during rift climax and reorganisation—Billefjorden Trough, Svalbard, Norway. *Basin Research*, 33(5), 1–32. <https://doi.org/10.1111/bre.12578>
- Statens havarikommisjon. (1989). Rapport om luftfartsulykke på Åsgårdsfonna, Svalbard, den 22. August 1987 med Aerospatiale AS 350 B1, LN-OMQ. Report on accident on Åsgårdsfonna, Svalbard, 22. August 1987 with Aerospatiale AS 350 B1, LN-OMQ (in Norwegian). Retrieved from <https://havarikommisjonen.no/Luftfart/Avgitte-rapporter/1989-07>
- Steel, R. J., & Worsley, D. (1984). Svalbard's post-Caledonian strata—An atlas of sedimentational patterns and palaeogeographic evolution. In *Petroleum geology of the North European margin* (pp. 109–135). Springer. https://doi.org/10.1007/978-94-009-5626-1_9
- Straume, E. O., Gaina, C., Medvedev, S., Hochmuth, K., Gohl, K., Whittaker, J. M., et al. (2019). GlobSed: Updated total sediment thickness in the world's oceans. *Geochemistry, Geophysics, Geosystems*, 20(4), 20–1772. <https://doi.org/10.1029/2018GC008115>
- Straume, E. O., Gaina, C., Medvedev, S., & Nisancioglu, K. H. (2020). Global Cenozoic Paleobathymetry with a focus on the Northern Hemisphere Oceanic Gateways. *Gondwana Research*, 86, 126–143. <https://doi.org/10.1016/j.gr.2020.05.011>
- ten Brink, U. S., Hackney, R. I., Bannister, S., Stern, T. A., & Makovsky, Y. (1997). Uplift of the Transantarctic Mountains and the bedrock beneath the East Antarctic ice sheet. *Journal of Geophysical Research*, 102(B12), 27603–27621. <https://doi.org/10.1029/97JB02483>

- Urlaub, M., Schmidt-Aursch, M. C., Jokat, W., & Kaul, N. (2009). Gravity crustal models and heat flow measurements for the Eurasia Basin, Arctic Ocean. *Marine Geophysical Researches*, 30(4), 277–292. <https://doi.org/10.1007/s11001-010-9093-x>
- Worsley, D. (2008). The post-Caledonian development of Svalbard and the western Barents Sea. *Polar Research*, 27(3), 298–317. <https://doi.org/10.1111/j.1751-8369.2008.00085.x>
- Zhao, S., Lambeck, K., & Lidberg, M. (2012). Lithosphere thickness and mantle viscosity inverted from GPS-derived deformation rates in Fennoscandia. *Geophysical Journal International*, 190(1), 278–292. <https://doi.org/10.1111/j.1365-246X.2012.05454.x>